Ore Geology Reviews 119 (2020) 103365

Contents lists available at ScienceDirect

Ore Geology Reviews

journal homepage: www.elsevier.com/locate/oregeorev

Mineralogical and isotope-geochemical ($\delta^{13}C$, $\delta^{34}S$ and Pb-Pb) characteristics of the Krasniy gold mine (Baikal-Patom Highlands): Constraining ore-forming mechanisms and the model for Sukhoi Log-type deposits

Yu.I. Tarasova[a,b,c,*], A.E. Budyak[a,c], A.V. Chugaev[d], N.A. Goryachev[a,g], V.L. Tauson[a], S.Yu. Skuzovatov[a], V.N. Reutsky[f], V.D. Abramova[d], B.I. Gareev[e], N.N. Bryukhanova[a], A.V. Parshin[a]

[a] Vinogradov Institute of Geochemistry, Russian Academy of Science, Siberian Branch, 1A Favorsky Str., Irkutsk 664033, Russia
[b] Irkutsk Scientific Center, Russian Academy of Science, Siberian Branch, 134 Lermontov Str., Irkutsk 664033, Russia
[c] Irkutsk National Research Technical University, 83, Lermontov Str., Irkutsk 664074, Russia
[d] Institute of Geology of Ore Deposits, Petrography, Mineralogy and Geochemistry, Russian Academy of Sciences, Staromonetnyi per. 35, Moscow 119017, Russia
[e] Kazan Federal University, 18 Kremlyovskaya Str., Kazan 420008, Russia
[f] Sobolev Institute of Geology and Mineralogy, Russian Academy of Sciences, Siberian Branch, 3 Koptyug Ave., Novosibirsk 630090, Russia
[g] Shilo North-Eastern Integrated Research Institute Russian Academy of Science Far-East Branch, 16 Portovaya Str., Magadan 685000, Russia

ARTICLE INFO

Keywords:
Gold ore deposit
Baikal–Patom belt
Metasedimentary rocks
Petrography
Mineralogy
Geochemistry
S, C, Pb, isotope composition
Organic matter

ABSTRACT

Orogenic gold deposits localized in carbonaceous sedimentary (black-shale) complexes are major contributors to worldwide balance of gold extracted from the crust, though there is a limited consensus about the role of host sedimentary rocks, involvement of external (i.e., magma-derived) fluids and brittle deformations into ore remobilization and transport. This paper presents the original results of mineralogical, petrographic and isotope-geochemical studies of rocks and ores from the large Krasniy gold deposit (Baikal-Patom plateau, southern Siberian craton) given in comparison with the thoroughly studied giant Sukhoi Log deposit, with both deposits hosted by the Neoproterozoic carbonaceous metasedimentary rocks. The multi-stage ore process occurred discretely at 200–400 °C (greenschist-facies metamorphism) and included (1) low-P-T diagenetic formation of globular pyrite, (2) catagenetic (< 200 °C, 1–2 kbar) formation of small euhedral pyrite, (3) high-temperature and high-pressure (300–380 °C, 5–6 kbar) crystallization of arsenopyrite and pyrrhotite related to metamorphic transformation, and (4) formation of the major ore assemblage (arsenopyrite, pyrrhotite, pyrite meta-aggregates, native gold, galena, sphalerite, fahl ores) during almost isothermal decompression (270–320 °C, 0.5 kbar). Gold is detected as nanoparticles unevenly distributed at the surface of the early globular pyrite (up to 0.4 ppm) and occurs as inclusions in later metamorphic pyrite. Relatively narrow ranges of sulfur ($\delta^{34}S$ within −4.7 – −6.9‰) and lead isotopic composition ($^{206}Pb/^{204}Pb$ = 18.33–18.65, $^{207}Pb/^{204}Pb$ = 15.65–15.68 and $^{208}Pb/^{204}Pb$ = 38.13–38.82) in sulfides from the ores was continuously inherited from earlier generation of sulfides to the later (associate with native gold) and is similar to the values obtained for sulfides from the host Neoproterozoic metasedimentary rocks of the Aunakit formation. The compositional inheritance together with geochemical evidence of no additional contribution of K, Na, Mg and Si into the ores and no correlation between gold and organic carbon content highlight the absence of the external metasomatic overprint of metal-bearing fluids. Instead, both the above facts and high Au content (up to 1 ppm) in bitumens derived from the host metasediments indicate a key role of the host carbonaceous substrate in the supply of metals through release and local transport of internally derived diagenetic/catagenetic carbon-rich fluids. Overall, the obtained results for the Krasniy deposit led to distinguishing the three key stages of the gold deposit formation, including 1) sedimentation of gold-specialized sediments in the spreading of the back-arc basin, where gold was associated with the scattered diagenetic pyrite mineralization (610–590 Ma), 2) catagenetic redistribution of sedimentary pore fluids from preconditioned sedimentary rocks into the vaulted parts of gentle anticlines with the formation of abnormally high concentrations of gold (~570 Ma), and 3) metamorphic-metasomatic redistribution of gold as a result of decarbonization of catagenic fluid with the formation of economically significant ore bodies

* Corresponding author at: Vinogradov Institute of Geochemistry, Russian Academy of Science, Siberian Branch, 1A Favorsky Str., Irkutsk 664033, Russia.
E-mail address: j.tarasova84@yandex.ru (Y.I. Tarasova).

https://doi.org/10.1016/j.oregeorev.2020.103365
Received 21 June 2019; Received in revised form 27 September 2019; Accepted 26 January 2020
Available online 11 February 2020

(450–420 Ma). The compilation of the available geochemical and isotopic data allows to suspect this model as a general for the other Bodaibo region deposits, so that it can be used further for prediction and exploration purposes.

1. Introduction

Orogenic gold deposits in accretionary belts are major sources of gold extracted at present from the crust (Groves, 1993; Goldfarb et al., 2005). Despite a great research interest over decades, there is still a limited consensus about the origin of such deposits, and particularly the role of metamorphic devolatilization and ore potential of sedimentary rocks (Connolly, 2010; Phillips and Powell, 2010; Tomkins, 2010; Zhong et al., 2015), involvement of external (i.e., magma-derived) fluids into ore remobilization and transport (Sillitoe and Thompson, 1998; Groves et al., 2003), as well as the role of brittle deformations and large-scale faults as conduits for pervasive fluids (Sibson et al., 1988; Gaboury, 2001; Cox, 2016). Regarding the worldwide balance of gold, a leading position belongs to deposits hosted by carbonaceous-terrigenous black-shale complexes due to the abundance and high ore potential of the latter (Groves et al., 2001; Large et al., 2011). Many large gold ore deposits, e.g., Bendigo, Kumtor, Sukhoi Log represent the orogenic type (Goldfarb et al., 2005; Groves et al., 2001), and their formation is closely related to development of orogenic fold belts. In addition, the issues on the ore sources and a possible role of the host black shales in ore-forming processes is a subject for long-lasting discussions (Kerrich and Cassidy, 1994; Groves et al., 1998; Large et al., 2007; Frei et al., 2009; Chugaev and Chernyshev, 2017).

The genesis of black-shale gold deposits discovered in the Lena Gold Province (LGP), one of the largest in Russia, has been differently grounded in the earlier studies (Safonov, 2003; Distler et al., 2004; Laverov et al., 2007; Large et al, 2007; Meffre et al., 2008; Yudovskaya et al., 2011; Yudovskaya et al., 2016; Palenova, 2015). Most researchers highlight the orogenic type of deposits, with locally recognized «Sukhoi Log» type, exemplified by the comprehensively studied Sukhoi Log giant deposit (Buryak et al., 2002; Nemerov et al., 2010; Wood and Popov, 2006; Large et al, 2007; Meffre et al., 2008; Palenova et al., 2015). This type involves gold deposits enclosed in the southern margin of the Siberian craton hosted by thick carbon-bearing continental-margin sediments and volcanogenic formations, which underwent intense collisional dislocations and zonal regional metamorphism (Buryak et al., 2002; Nemerov et al., 2010). Within LGP, the veinlet-impregnated and stockwork bodies (e.g., in the Sukhoi Log, Golets Vysochaishy, Verninsky deposits) and large gold-quartz veins (in the Ozherelie, Dogaldyn, and Kopylovsky deposits) are the principal gold ore units (Ivanov, 2014). Some researchers assumed that all large deposits in the region commonly formed through voluminous plume-related magmatism and granite formation (Rundquist, 1997; Distler et al., 2004; Laverov et al., 2007). The accepted postmagmatic-hydrothermal concept based on the key role of intrusive granitoid magmatism (Kazakevich et al., 1971; Lishnevskii and Distler, 2004) postulates that hydrothermal solutions and deep-seated gas flows contributed notably to the ore formation (Laverov et al., 1997, 2007; Rundquist, 1997; Safonov, 2003). In contrast, the metamorphic-hydrothermal model suggests that the main components of ores originate from the host black-shale sequences (Buryak et al., 2002; Vilor et al., 2003; Nemerov and Stanevich, 2001; Dubinina et al., 2014; Meffre et al., 2008; Large et al., 2007; Chugaev and Chernyshev, 2017). This alternative model is consistent both with mineralization controlled largely by the zonal regional metamorphism, folded anticlines and adjacent zones of schistosity, and numerous isotopic evidences of the host rock involvement into the ore-forming processes (Chugaev et al., 2017, Chugaev et al., 2018) and its later remobilization during the Early Paleozoic

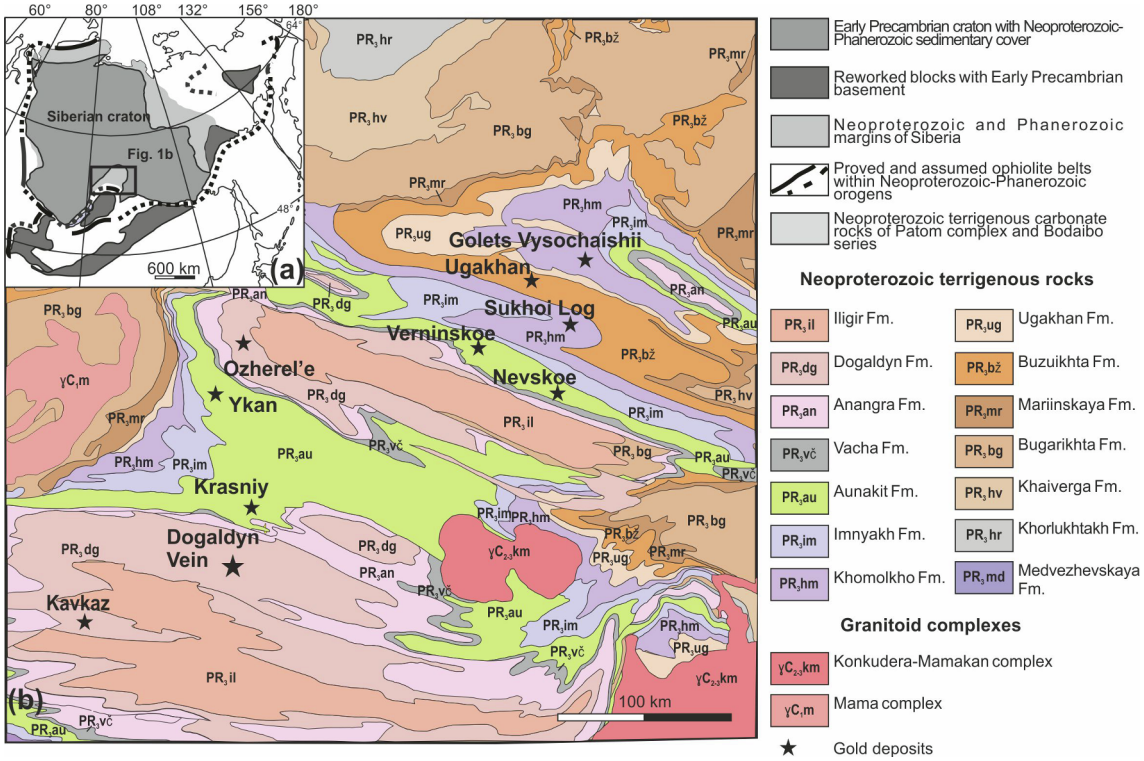

Fig. 1. (a) Simplified tectonic structure of the northeastern Asia with the relative position of the Siberian craton and major microcontinental blocks (after Skuzovatov et al., 2019a, Skuzovatov et al., 2019b); (b) Geological structure of the Mama-Bodaibo zone within the Baikal-Patom belt and location of gold deposits (Gold, 2010).

accretionary tectonics (Nemerov and Stanevich, 2001; Budyak et al., 2016; Budyak et al., 2017).

The long-term investigations provided an essential bulk of geological, mineralogical, geochemical and geochronological data mostly for the giant Sukhoi Log deposit (Distler et al., 1996; Buryak and Khmelevskaya, 1997; Laverov et al., 2007; Meffre et al., 2008; Yudovskaya et al., 2011, 2016; Kryazhev et al., 2009; Chernyshev et al., 2009). As to the other deposits, the available data are sparse (Martynenko et al., 2017; Chugaev et al., 2014; Rusinov et al., 2008; Vagina, 2012; Kucherenko et al., 2012). Determination of general and individual mineralogical and geochemical (including isotopic) signatures of Sukhoi Log-type deposits is undoubtedly essential to develop a general genetic model. This is particularly vital for recognizing the contribution of organic substances of host rocks to mobilization, transfer and concentration of gold by hydrothermal solutions while interacting with the carbonaceous sequences. This paper yields original data on the mineralogy and geochemistry of host rocks and ores, isotope geochemistry of lead and sulphur in ore minerals, as well as isotope composition of carbon of the organic substance of ore-hosting sequences of the large Krasniy gold deposit (1.3 Mt of Au, internal assessment of the GV GOLD mining company).

2. Regional geological setting

The Krasniy gold deposit is located in the Baikal-Patom Highlands, Irkutsk Region of Russia, within the Bodaibo synclinorium enclosing most of gold ore deposits (Fig. 1a) (Ivanov, 2014). The Neoproterozoic terrigenous-carbonate sediments make up the Medvezhevsky-Balaganakh, Dal'naya Taiga, Zhuya and Yudoma groups reflecting four large-scale sedimentation cycles. The sedimentary sequences consist of the horizons of calcareous rocks intercalated with phyllite-like shales and metasediments (Fig. 2) (Budyak et al., 2015a, 2015b; Chugaev et al., 2018; Nemerov et al., 2010; Stanevich et al., 2007a, 2007b; Palenova et al., 2019). The paleotectonic reconstructions show that the sediments of the Medvezhevsky-Balaganakh group accumulated in the open oceanic basin related to passive-margin setting of the Siberian Craton. The paleobasin was initiated as a response to continental margin rifting triggered by the Rodinia supercontinent break-up in the early Neoproterozoic (790–740 Ma) (Li et al., 2008; Bogdanova et al., 2009; Gladkochub et al., 2013). The overlying Ediacarian sediments of the Dal'naya Taiga – Zhuya (635–580 Ma) and Yudoma groups (580–540 Ma) (Melezhik et al., 2009; Yudovskaya et al., 2011; Kuznetsov et al., 2013; Gladkochub et al., 2013; Chumakov et al., 2011, 2013; Powerman et al., 2015; Pokrovsky and Bujakaite, 2015) deposited throughout the evolution from back-arc basin to the foreland basin (Gordienko and Mironov, 2008; Zhmodik et al., 2006; Nemerov et al., 2010; Chugaev et al., 2017, Chugaev et al., 2018) owing to accretion of the Baikal-Muya terrane to the Siberian continent (summarized recently by Skuzovatov et al., 2019a, Skuzovatov et al., 2019b). Due to the Early Cambrian metamorphism (520–555 Ma; Vinogradov et al., 1996; Scott et al., 2007), the metasediments folded into large linear and arc-like folds of sublatitudinal direction (Buryak and Khmelevskaya, 1997; Yudovskaya et al., 2011), with minor folding of higher orders and widespread brittle deformations. This led to rise of the Bodaibo zone in the central part of the Baikal-Patom Province (BPP), bounded from the south by exposures of Paleozoic granitoids of

Age, Ga	Group	Formation	Characteristics of host rocks		Thick, m	Bodaibo syncline composite	
						Bodaibo syncline	Marakan–Tunguska syncline
540	Yudoma	Iligir	arkosic metasandstone with smallthickness layers of sericite-chlorite shales		600-1000		
		Dogaldyn	polymictic sandstones and shales with a large amount of volcanic rokcs		400-800	Kavkaz, Kopylovskoe, Dogaldyn vein	Ozherel'e, Rodnikovy
		Anangra	gravelites, polymictic sandstones sericite-chlorite shales		50-500		
580	Zhuya	Vacha	quartz-sericite shales		100-300		
		Aunakit	quartz, calcareous sandstones with layers of calcareous aleurolites and carboniferous shales		> 900 м	Krasniy	Verninskoe, Nevskoe, Ykan, Shushkukan
		Imnyakh	calcareous aleuroshales, carbonate-micaceous shales, marl		300-800		
	Dal'nyaya Taiga	Khomolkho	dark grey carboniferous phyllitic and carbonaceous-sericite-quartz microshales		500-1100		Sukhoi Log, Golets Vysochaishii
610		Ugakhan	carbonaceous biogenic limestones with smallthickness layers of carboniferous shales		200-1100		
		Buzhuikhta	quartz sandstones and arbonaceous plagioclase-sericite-chlorite-quartz shales		400-1200		Ugakhan
635	Balaganakh	Mariinskaya	gray layered limestone with an admixture of terrigenous material and organic matter		100-300		
		Bugarikhta	sequence of oligomictic and arcosic sandstones with shales		300-500		
		Khaiverga	sequence of shales and oligomictic at least arkosic sandstone and aleurolites		400		
~770		Khorlukhtakh	polymictic and feldspar-quartz gravelites and sandstones with lesser extent dark-gray carbonaceous shale.		300-800		

Fig. 2. The generalized stratigraphic scheme with location of the Bodaibo synclinorium deposits. Compiled using materials and geochronological estimates from Melezhik et al. (2009), Yudovskaya et al. (2011), Kuznetsov et al. (2013), Chumakov et al. (2013), Pokrovskiy and Buyakaite (Pokrovsky and Bujakaite, 2015), and Powerman et al. (2015).

the Angara-Vitim batholith and – from the north – by the Baikal and Lena system of marginal troughs and the Chuya, Tonod and Nechera uplifts.

The Bodaibo zone incorporates folded structures of the second order, Marakan-Tungusska and Bodaibo synclines, separated by the Kropotkin anticline (Fig. 1b). The Bodaibo synclinorium is specified by the presence of metamorphic zonation exhibiting crystalline schists of amphibolite and epidote–amphibolite facies over the synclinorium margin and poorly metamorphosed rocks of greenschist facies in its central part. Numerous gold deposits occur within poorly metamorphosed rocks (Fig. 2). The regional metamorphism here peaked in the Late Silurian-Ordovician (~450–420 Ma); it was linked with the accretion and coeval S-type granites of the Mama complex (Zorin et al., 2008) in the south of the Siberian Craton. The younger, Hercynian granitoid intrusions of the Konkudera-Mamakan complex (Yarmolyuk et al., 1997; Tsygankov et al., 2007, Tsygankov et al., 2010) related to the Angara-Vitim batholith activity (Bukharov et al., 1992; Neymark et al., 1993; Tsygankov et al., 2010).

The deposits of the Bodaibo synclinorium are confined to the Dogaldyn (Yudoma group), Aunakit and Khomolkho (Dal'naya Taiga and Zhuya groups) formations (Fm) (Fig. 2). The large-scale mineralization (Sukhoi Log and Verninsky deposits) has been recognized only in sedimentary sequences of the Khomolkho and Aunakit Fm, which accumulated in a semi-closed (foreland) basin (Nemerov et al., 2010; Budyak et al., 2016; Chugaev et al., 2017, Chugaev et al., 2018).

3. Geology of the Krasniy gold deposit

The Krasniy gold deposit is enclosed in the Aunakit Fm of the Zhuya group (Fig. 2). Terrigenous sediments of this formation making up the intercalated horizons of C-bearing (C_{org} up to 4 wt%) metasediments and siltstones concordantly overlie carbonate rocks of the Imnyakh Fm. Within the deposit, the total thickness of sediments reaches 1000 m; it incorporates five bedded sequences making up three subformations. At the top of the section, the rocks are overlapped by carbonaceous (C_{org} = 10 wt%) quartz-sericitic shales interbedded with carbonaceous quartz sandstones of the Vacha Fm. The total thickness of sediments is about 300 m. The upper part (au_3) exhibits intercalated dark grey to

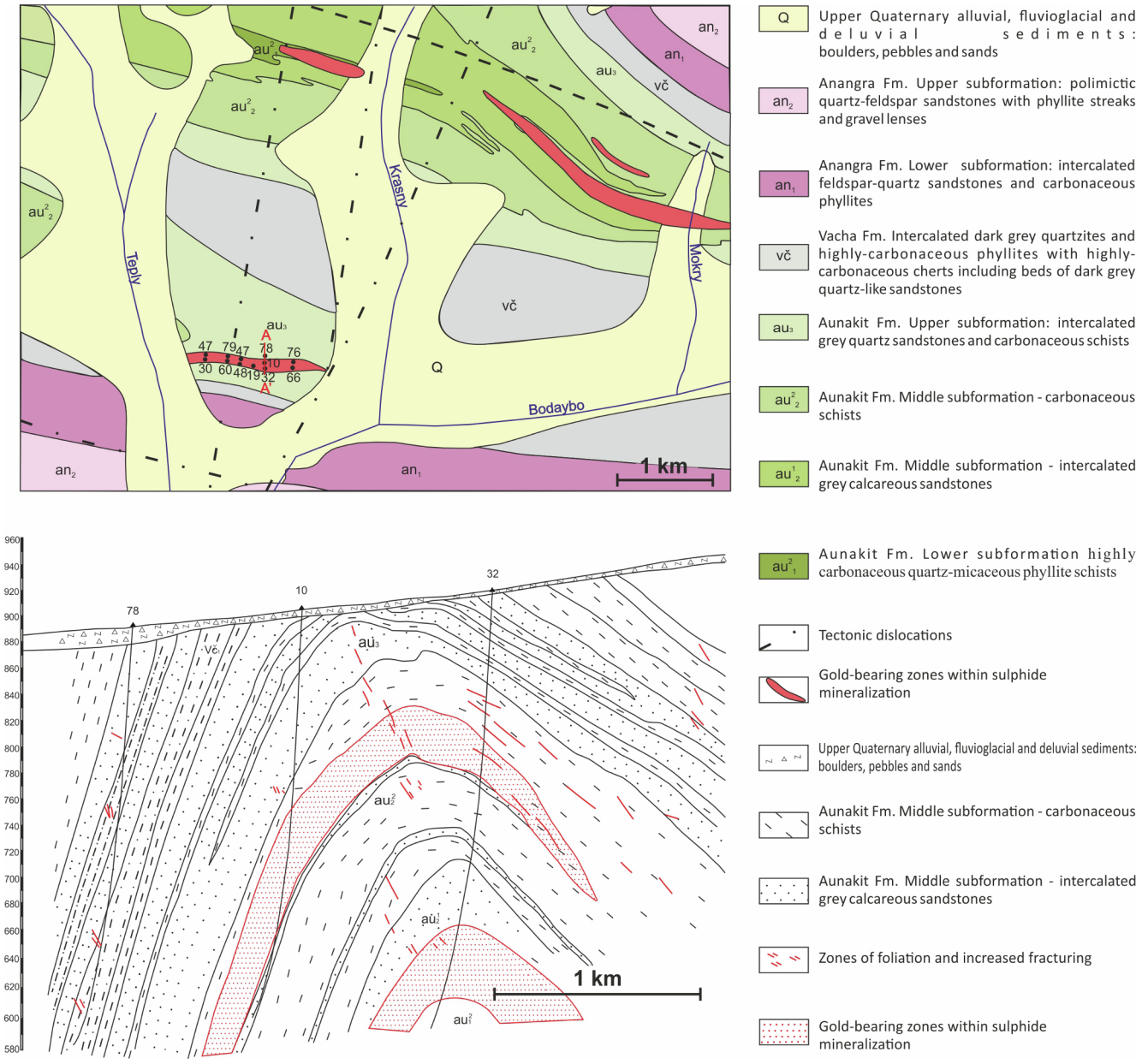

Fig. 3. Geological structure of the Krasniy ore field: a – schematic map; b – schematic cross-section through the deposit along the A-A' line.

black silty-quartz and oligomictic sandstones and marks the horizon between black shales of the Vacha Fm (vc) and au_2^2. Within the middle subformation, the upper sequence (au_2^2) contains highly carbonaceous quartz-micaceous phyllite schists, whereas the lower sequence (au_2^1) contains dark grey quartz, oligomictic, rarely calcareous silt- and sandstones. In the lower subformation, the upper sequence (au_1^2) is composed of highly carbonaceous quartz-micaceous phyllite schists, and the lower one (au_1^1) consists of rhythmically intercalated quartz and oligomictic calcareous sandstones with mica-quartz silty and calcareous-micaceous shales.

The hosting metasedimentary sequences underwent plastic deformations, which produced high-order linear folds complicated by numerous low-amplitude syn-fold and late-fold dislocations similar to shear upthrusts and fault overthrusts. Longitudinal, sublatitudinal and diagonal zones of enhanced fracturing are widespread. The largest folded structures are the third order anticline folds Rudnaya and Verkhne-Bodaibo separated by the Lozhkovaya syncline (Fig. 3). The anticline hosting gold ore mineralization is an upturned fold striking southeast, with the axial plane dipping northeast at 70°–85°. The limbs comprise bedded sequences of intercalated sandstones and phyllites reaching 60 m in thickness. The anticline is ubiquitously complicated by higher order dislocations, e.g. primarily small folding, shear zones and cataclasis of rocks.

The deposit host two ore bodies: the upper one extending for 1100 m, 60 m thick, and the lower one extending for 1440 m and 90 m in thickness. As the ore bodies do not show any distinct geological boundaries, they were recognized from available sampling results. In the cross-section, the bodies are saddle-shaped, and they are constrained by the anticline fold hinges. Thick ore bodies as well as swells are observed in the dome part of folds and close to plicative structures (Palenova, 2015). The ore bodies occur different bedded sequences of the Aunakit Fm (Fig. 3b). The upper ore body (OB-1) lies on the contact of rocks of silt-and-sandstone sequence with stringers of carbonaceous schists of the upper subformation (au_3) and highly carbonaceous black shale sequence, middle subformation of the Aunakit formation (au_2^2). The lower ore body (OB-2) occurs at the contact of siltstone-sand sequence of the middle subformation (au_2^1) with rocks of highly carbonaceous black shale sequence (au_1^2), lower subformation. Barren zones or poorly mineralized rocks separate the ore bodies. The thickness of barren zones reaches the first tens of meters. The entire sequence of host rocks is sulfidized. However, close to the ore bodies the degree of silicification, carbonation and sulfidation increases. The ore bodies are commonly typified by the mineral associations: (1) dispersed sulfide mineralization of fine idiomorphic pyrite crystals occurring throughout the ore field (Fig. 4a); (2) veinlet-impregnated (Fig. 4 b) pyrite and pyrrhotite mineralization; (3) quartz-sulfide mineralization with veinlets of milky-white quartz with cubic pyrite, which are differently oriented in space and often cross the ore bodies (Fig. 4c); and (4) thick veins of brownish quartz without any visible sulfide mineralization (Fig. 4d). This paper reports only the veinlet-impregnated type of ores, as gold is not associated with any other types.

4. Analytical methods

The mineralogy and petrography of rocks and ores collected from outcrops and drill cores was examined using optical microscopes Polam-3, Polam-2 and Olympus BX-51 (total of 300 thin sections). The composition of major ore minerals, including Au content and speciation, in the upper and lower bodies were analyzed by EPMA using JXA8200 electron-microprobe analyzer (JEOL Ltd. Company)

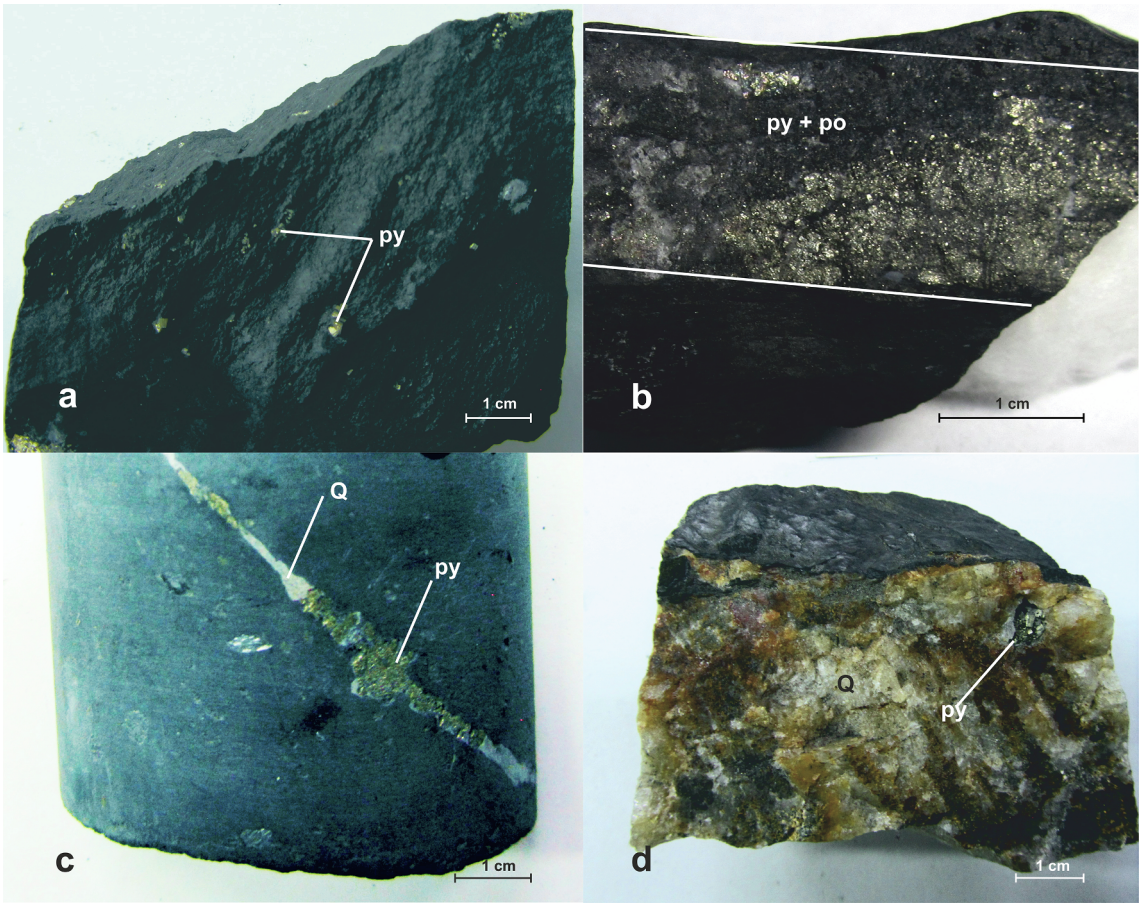

Fig. 4. Major types of mineralization distinguished at the Krasniy deposit: (a) dispersed idiomorphic pyrite crystals, (b) a veinlet with pyrite and pyrrhotite, (c) veinlets of milky-white quartz bearing fine cubic pyrite, (d) a vein of brownish quartz with pyrite pocket.

(performed by L.A. Pavlova). The analysis was conducted at accelerating voltage of 20 kV and probe current of 25nA. For the quantitative analysis of microinclusions with the raster microscope employed, the resolution was equal to 3–5 μm.

Trace-element content of sulfides, including Au content, involved two independent procedures based on laser ablation inductively coupled mass-spectrometry technique (LA-ICP-MS). At the first stage, concentrations of ^{33}S, ^{51}V, ^{57}Fe, ^{59}Co, ^{60}Ni, ^{65}Cu, ^{66}Zn, ^{75}As, ^{77}Se, ^{107}Ag, ^{121}Sb, ^{197}Au and ^{209}Bi in pyrite and arsenopyrite were analyzed at the Center "IGEM-analitika" of IGEM RAS. The LA-ICP-MS system employed a New Wave UP-213 solid-state Nd:YAG laser coupled with an Thermo XSeries2 quadrupole ICP-MS. Measurements were conducted on 40–60 μm spots and raster lines (7 μm/s ablation speed for lines), with a laser frequency of 15 Hz and resulting 5–7 J/cm^2 energy density. The carrier gas consisted of a mixture of He (0.75 L/min) and Ar (0.85 L/min). The acquisition scheme in a spot mode was 30 s for the blanks, 60 s for the mineral analysis and 30 s washout time. Each line profile was preceded by 30 s of blank analysis. The ICP-MS operated in a time-resolved mode using peak jumping and a dwell time of 10 ms/peak per element. Signal quantification was carried out by Iolite software using ^{57}Fe as an internal standard. For external calibration the standard reference materials (SRM) UQAC FeS_{-1} (University of Quebec in Chicoutimi, Canada), produced from natural sulfide powder and doped with trace elements, was used. The MASS-1 polymetal sulfide (USGS) was used for verification of the results.

In more detail, the Au contents, as well as its distribution patterns in some pyrite grains were assessed by another LA-ICP-MS system based on a Agilent 7500ce quadrupole mass-spectrometer (Agilent Technologies, the USA) and a New Wave Research UP-213 LA platform (the Center for Collective Use «UltraMicroAnalysis», Institute of Limnology, Irkutsk). The sieve fraction of grains used for analyses varied from −1 to +0.5. The Au and As concentrations were estimated relative to the SRM NIST 612 silicate-based standard glass. The analytical uncertainties and reproducibility were checked by repeated analysis of the MA4-1 laboratory standard (synthetic crystal of greenockite, CdS) with homogeneously distributed Au primarily in the structural form (Tauson, 1999; Tauson et al., 2015).

The contents of 10 major oxides in rock powders (< 0.02 mm) were determined by X-Ray Fluorescence (XRF) method using a Bruker S4 Pioneer XRF spectrometer. All samples were preliminarily annealed in the muffle furnace at temperature 650°C during 3 h to remove sulfur, and then fused with Li-metaborate in the induction furnace at 1100 °C. Losses on ignition (LOI) were defined in the initial material at T = 950 °C in the muffle furnace. The analyses were performed with Rh anode, voltage of 30 kV and of 40 mA current (Afonin et al., 1984). The SGD-1A (gabbro), ST-1A (trapp), SG-1A (granite), SG-2 (granite), SA-1 (siltstone), SI-2 (carbonatite), SDU-1 (dunite) (Russia), JB-1 (basalt), and JP-1 (peridotite) (Japan) reference materials were repeatedly used as standards. Trace-element analysis was performed using the ICP-MS method, which utilized the technique reported in detail by Skuzovatov et al. (2018). The rock powders (100 mg each) were fused with dry Li metaborate (1:4) in carbon crucibles, and then decomposed in a mixture of distilled HF and HNO_3. Trace element ICP-MS analyses were performed using a Agilent 7700 quadrupole mass-spectrometer (Agilent Technologies) at the Baikal Center of Nanotechnologies based at the Irkutsk Ikutsk National Research Technical University (Irkutsk, Russia). For both XRF and ICP-MS analyses, corresponding analytical uncertainties were within 5%.

The Au and Ag contents in ores and host sediments were analyzed by scintillation and atomic absorption analyses using Perkin-Elmer M−303 and Perkin-Elmer M−405 atomic-absorption spectrometers measured (performed by V.N. Vlasova), with a preliminary extraction of sulfides with oil (Torgov and Khlebnikova, 1977). Corresponding detection limits for the two spectrometers were 0.005 and 0.002 ppm, respectively.

The primary fluid inclusions 15 μm or more in size were examined in the two-sided polished quartz plates (0.3–0.5 mm thick) by the methods of thermobarometry and Raman spectroscopy. The temperatures of total homogenization, eutectics and ice melting of solutions were measured by the Linkam THMSG-600 microthermal chamber installed on the Olympus BX-51 microscope. The temperature interval of phase transitions ranged from –196 to +600 °C. The accuracy of measurements was ±0.1 °C in the range from –20 to +80 °C, and ±1 °C beyond that interval. The calculations were made using LinkSys V-2.39 software. Salinity of mineral-forming solutions was estimated by the Flincor program (Brown, 1989) for the NaCl-H_2O-CO_2 system. The composition of a liquid phase in inclusions was determined based on the temperatures of eutectics characterizing the water-salt system.

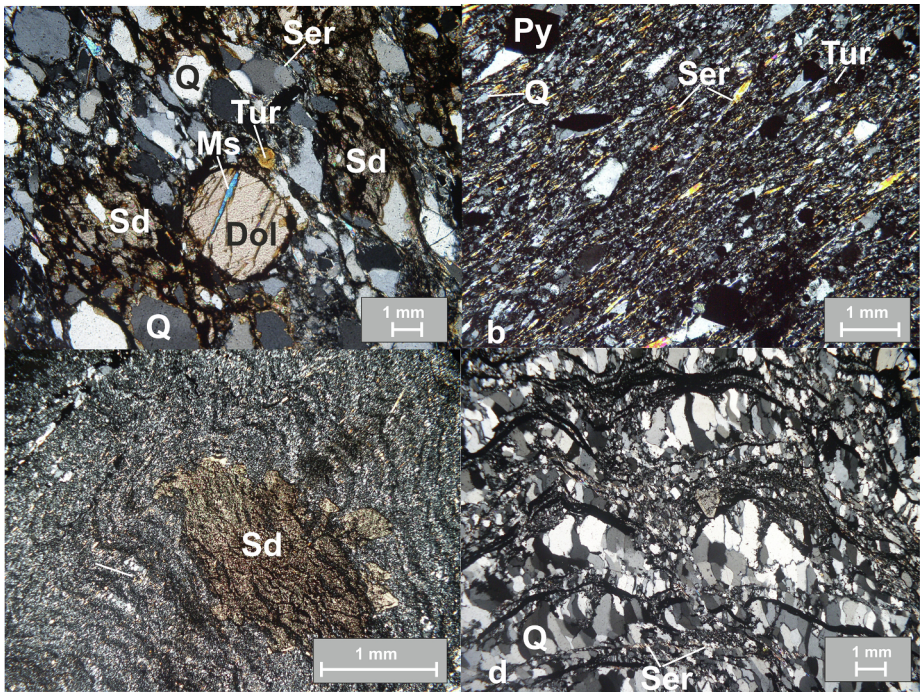

Fig. 5. Representative microphotographs of petrography of the Krasniy deposit host rocks: a – a dolomite grain with a muscovite plate in newly formed siderite replacing the sandstone cement; b – black highly carbonaceous schists containing abundant carbonaceous substance and pyrite impregnations with secondary quartz; c – highly carbonaceous microshale of sericite-quartz composition with carbonate porphyroblasts, fine pyrite phenocrysts and a thin pyrite-quartz veinlet; d – a veinlet of carbonaceous sericite-quartz schist with banding and plating.

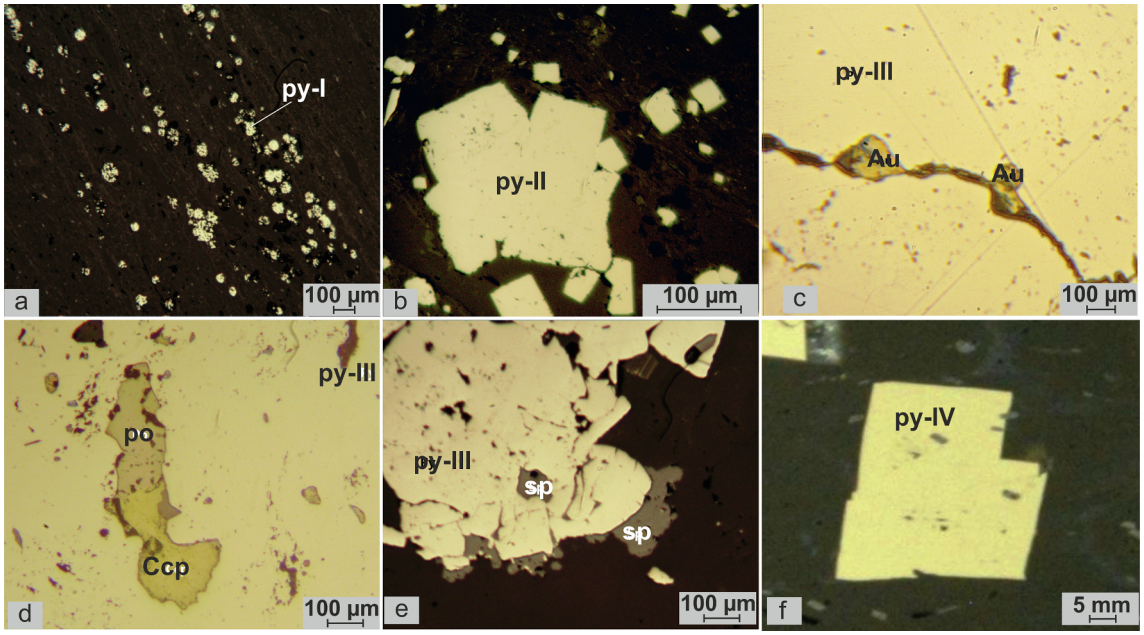

Fig. 6. Morphological varieties of pyrite: a – banded cluster of thin impregnated aggregates of framboidal pyrite-I; b – fine idiomorphic crystals of pyrite–II; c – gold inclusions through fracture in pyrite-III; d – joint aggregates of pyrrhotite and chalcopyrite over pyrite–III rim; e – sphalerite inclusions in pyrite-III and over its edge; f – pyrite-IV crystal.

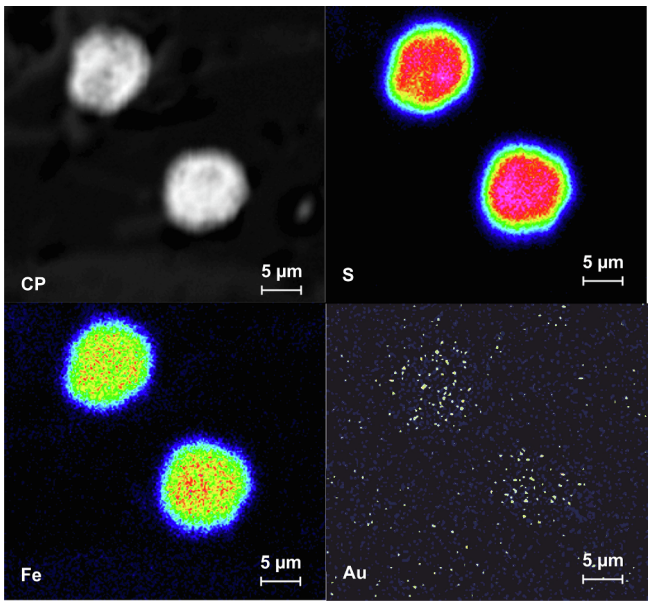

Fig. 7. Distribution of the X-ray radiation intensity from selected elements in framboidal pyrite-I.

Salinity of a water phase in inclusions was determined after the ice melting temperature through equivalent in the NaCl-H_2O system (Bodnar and Vityk, 1995). The phase composition of a gas phase of fluid inclusions was evaluated using the Raman spectrometer Horiba Lab Ram HR 800 (IGM SB RAS, Novosibirsk).

The Pb isotope composition of pyrite was analyzed in 0.02–0.05 g single-mineral fractions. The samples were chemically treated at IGEM RAS with the techniques described earlier (Manhes et al., 1984; Chugaev et al., 2013). The Pb isotope composition was measured at the Laboratory of isotope geochemistry and stratigraphy by a NEPTUNE PLUS multi-collector mass-spectrometer (ThermoFinnigan, Germany) (Chernyshev et al., 2007). The Pb, Th and U contents were determined using a quadrupole X-7 ICP-MS mass-spectrometer (Thermo Elemental, the USA) in the same solution samples traced by indium.

The organic matter of rocks was processed through multi-stage procedure, which included separation of asphaltenes and asphaltenic/asphalt-generating acids insoluble in petroliferous ether and further chromatographic elution of the residue (Martikhaeva et al., 2001). The weighted samples of bitumens were dissolved in a small volume of benzene with the addition of petroliferous ether, and kept further in a dark place. The solution with a precipitated residue was then run through a chromatographic column, where asphaltenes and asphalt-generating acids remained on the absorbent, and a mix of hydrocarbons, benzene and alcohol-benzene resins was cleaned with petroliferous ether after release from the column. The asphalt-generating acids were washed out from the cotton with hot ethanol, and asphaltenes were washed with chloroform. A mix of hydrocarbons, benzene and alcohol-benzene resins received at the exit from the first column was laid over the second column filled with silica gel. Hydrocarbons were washed out with petroliferous ether, whereas benzene resins were washed with benzene, and alcohol-benzene resins with alcohol-benzene. The resultant eluates were concentrated on the rotary evaporator to be dried to a constant mass.

For analysis, the weighed sample of bitumen was dissolved in chloroform mixed with ethanol. The reference sample for controlling the data quality was prepared from the aqueous solution containing 100 μg/ml Ag, Au, As, Co, Cu, Mn, Mo, Ni, Pb, V and Zn by mixing aqueous solution with ethanol and chloroform. The graduation solutions were prepared by dissolving of sample for comparison with the 1 μg/ml content of elements in a mix of chloroform and alcohol. The analysis is performed by atomic-absorption spectrophotometer Perkin-Elmer 503 with electrothermal atomization (Vall and Voropaeva, 1982).

Carbon and sulfur isotope analyses were done in the Center for multi-elemental and isotope analysis (Institute of Geology and Mineralogy SB RAS, Novosibirsk). For bulk carbon isotope analysis, carbon was extracted from up to 1 g of each sample through oxidation of a powdered rock in a vacuumed reactor tube made of a fused quartz. The procedure employed a purified copper oxide as an oxidizer. The reactor containing mix of sample and CuO was pumped out down to the pressure of 10^{-4} Pa and then heated up to 950 °C for 20 min. Resulting

Table 1
Trace-element composition of pyrite of different generations at the Krasniy deposit determined by LA-ICP-MS (ppm).

Point	V	Cr	Co	Ni	Cu	Zn	As	Se	Ag	Sb	Au	Bi
py-I	–	–	0.36	126	–	–	1420	–	0.11	–	0.12	1.09
py-I	–	–	7.57	79.0	–	–	2420	–	–	–	0.15	–
py-I	–	46.0	0.80	18.7	6.45	–	1220	–	0.10	–	0.12	–
py-II	–	42.0	0.78	31.0	4.00	2.24	1126	–	0.07	–	0.17	–
py-II	–	5.30	9.90	539	13.2	–	99.0	–	0.29	–	0.11	1.52
py-II	–	140.0	3.50	920	7.60	–	2250	–	0.18	0.68	0.40	–
py-III	–	–	0.43	193	40.7	–	283	–	–	–	–	–
py-III	–	–	0.33	41.5	–	–	1820	–	–	–	–	–
py-III	–	3.40	79.80	614	2.90	–	2790	–	–	–	–	–
py-III	1.65	–	0.61	649	2.90	–	3130	–	0.87	0.87	–	3.93
py-III	–	81.0	1.01	692	4.63	3.70	1780	50.0	0.23	0.28	–	1.63
py-IV	–	36.0	–	3.74	3.32	–	1256	56.0	0.17	–	–	–
py-IV	–	–	–	–	–	–	221	77.0	0.14	–	–	–
py-IV	–	–	0.31	4.72	–	–	865	–	–	–	–	–
py-IV	–	–	–	–	–	–	214	16.0	–	–	–	–

Note: For Hg, Pb, Zn, Cu, Sb, Ti, Co, «-» is designated for contents below detection limits.

Table 2
LA-ICP-MS data for Au content in pyrite-I and pyrite-II of the Krasniy deposit.

Sample number		Au^{197}, ppm		
		n*	average	Mean square deviation,%
KR-4	py-I	2	0.60	68
	py-II	5	0.57	70
KR-9	py-I	3	1.16	78
	py-II	4	1.20	75
KR-10	py-I	3	0.80	49
	py-II	10	0.84	52
KR-14	py-I	4	0.42	40
	py-II	8	0.56	51
KR-16	py-I	4	0.69	54
	py-II	4	0.73	50
KR-18	py-I	5	0.71	62
	py-II	7	0.77	58
KR-19	py-I	4	0.63	68
	py-II	11	0.61	75
KR-30	py-I	3	0.47	64
	py-II	6	0.50	67
KR-39	py-I	2	0.74	54
	py-II	4	0.80	57

Note: n* is a number of analyses, in which the Au content was at or above DL ($C_{Au} \geq 0.2$ ppm).

carbon dioxide was purified and transferred to a detachable glass vial. Measurements of the carbon isotope composition were performed using a Delta V Advantage gas source mass-spectrometer in a dual inlet mode. The reproducibility of the carbon isotope measurements, including the sample preparation procedure, is better than 0.1‰. The USGS-24 standard (graphite with $\delta^{13}C = -15.9‰$ PDB) was used to control the isotope analysis procedure. All the $\delta^{13}C$ values are given in relation to the VPDB standard. Sulfur isotope analyses involved a procedure reported by Palyanova et al. (Pal'yanova et al., 2016). Samples of monomineral fractions (10–15 mg) were mixed with vanadium oxide and quartz sand in a 1:10:10 proportion and packed into glass vessels made of fused quartz as suggested by Han et al. (2002). The vessels were pumped out down to 10^{-4} Pa and baked at 450 °C for 30 min with pumping, then heated up to 850 °C for 30 min to complete sample combustion. Measurements of the sulfur isotope composition were performed using an isotope mass-spectrometer Delta V Advantage instrument in a dual inlet mode. The data was controlled by a set of reference materials with known $\delta^{34}S$ values: IAEA-S-1 (silver sulfide $\delta^{34}S = -0.3$), IAEA-S-2 (silver sulfide $\delta^{34}S = +22.7$), IAEA-S-3 (silver sulfide $\delta^{34}S = -32.3$) and NBS-123 (sphalerite $\delta^{34}S = +17{,}44$). Reproducibility of $\delta^{34}S$ values including sample preparation is better than 0.1‰ (2σ). The $\delta^{34}S$ values are given in relation to the CDT reference material (Canyon Diablo Troilite). The analytical data from the above

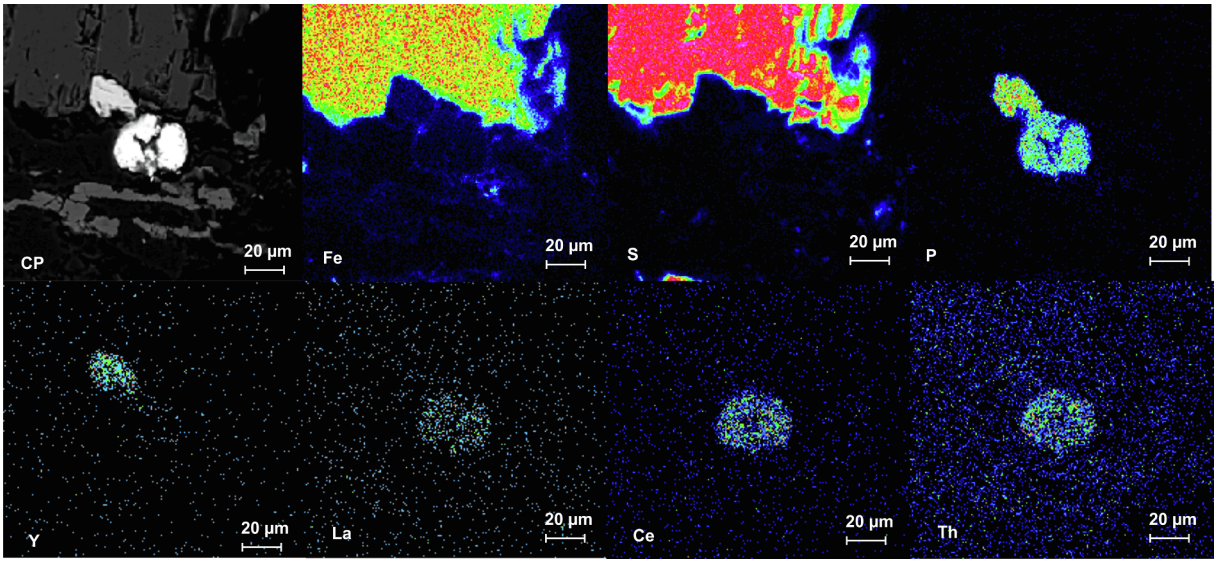

Fig. 8. The aggregate of xenotime and monazite within the crack in pyrite-III. Distribution of the X-ray radiation intensity of the elements by EPMA.

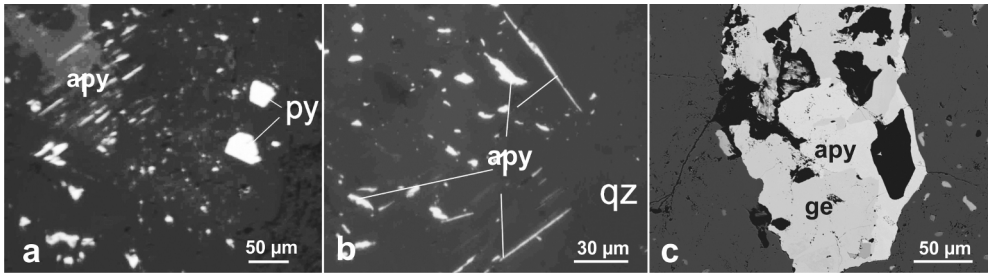

Fig. 9. Back-scattered images of arsenopyrite (apy) and gersdorffite (ge) occurrences: a – thin needle-shaped crystals of arsenopyrite-I in the host-rock matrix; b – aggregates of arsenopyrite-II and gersdorffite.

Table 3
Major element composition of the Krasniy deposit ore minerals from distinct mineral assemblages.

Mineral associations	Point number	Compositions and formulas						
		Sphalerite, mol. %			Arsenopyrite		Pyrrhotite	
		FeS	CdS	CuS	Formula	At. %As	Formula	At. %Fe
Gn, Sph, Cpy, Py-III	8t t3	0.9	2.6	–	–	–	–	–
	8t t6	2.3	2.4	–	–	–	–	–
	10t t3	0.8	3.0	–	–	–	–	–
Fahlore,Gn,Sph,Py-III, Cpy,Qz	16t t7	3.1	2.4	–	–	–	–	–
	16t t4	2.8	1.6	1.5	–	–	–	–
	16t t16	4.9	5.3	1.9	–	–	–	–
Fahlore,Sph,Cpy, Py-III, Po-II,Gn	10 t tvkl	3.3	3.4	–	–	–	–	–
	10t t4	–	–	–	–	–	$Fe_{0.80}S$	47.1
	10t t6	–	–	–	–	–	$Fe_{0.80}S$	44.4
Fahlore,Sph,Cpy,Py-III, Gn	16t t1	3.9	3.0	–	–	–	–	–
	16t t6	4.9	0.9	–	–	–	–	–
	" t12	6.3	2.3	–	–	–	–	–
Asp-II,Cpy,Sph,Gn, Py-III, Po-II,Au,Zc	7t t2	7.4	4.0	–	–	–	–	–
	t1	3.8	3.2	–	–	–	–	–
	t1	–	–	–	$FeAs_{1.22}S_{1.2}$	35.7	–	–
	t3	–	–	–	$FeAs_{1.28}S_{1.31}$	35.6	–	–
	t4	–	–	–	$FeAs_{1.23}S_{1.24}$	35.4	–	–
	7t t3	–	–	–	$FeAs_{1.16}S_{1.12}$	35.4	–	–
	t7	–	–	–	–	–	$Fe_{0.802}S$	44.5
Fahlore, Gn, Sph,Cpy,Py-III	11t t2	3.1	1.7	3.4	–	–	–	–
	11t t4	3.3	9.0	3.7	–	–	–	–
	" t4-1	4.4	10.6	4.1	–	–	–	–
Cb*,Sph,Cpy,Gn, carbonates	13t t4	1.0	1.9	–	–	–	–	–
Asp-II, Py-II,Po-I, Cpy, Fahlore, Zc	?	–	–	–	$FeAs_{1.21}S_{1.16}$	35.9	–	–
	7t t1	–	–	–	$FeAs_{1.23}S_{1.16}$	36.3	–	–
	7t t3	–	–	–	–	–	$Fe_{0.879}S$	46.8
	" t5-1	–	–	–	–	–	$Fe_{0.833}S$	45.4
Sph,Cpy, Py-III, Asp-II, Po-II, Au, Gn, Pn, Gf	15t t6	7.4	–	–	–	–	–	–
	t4	–	–	–	$FeAs_{1.20}S_{1.17}$	35.6	–	–
	7t t1	–	–	–	$FeAs_{1.20}S_{1.16}$	35.7	–	–
	15t t4	–	–	–	–	–	$Fe_{0.80}S$	44.4
	15t t7	–	–	–	–	–	$Fe_{0.817}S$	45.0
	15t t8	–	–	–	–	–	$Fe_{0.835}S$	45.5
	" t14	–	–	–	–	–	$Fe_{0.85}S$	45.9
	7t t4	–	–	–	–	–	$Fe_{0.806}S$	44.5
	" tvkl	–	–	–	–	–	$Fe_{0.833}S$	46.1
Py-II, Po-I, Asp-I, Cpy, Mt, Wu?, Qz, Mon,Gt?**	z2	4.5	2.1	–	–	–	–	–
	16t t7	–	–	–	$FeAs_{0.99}S_{0.82}$	35.1	–	–
	14 t	–	–	–	–	–	$Fe_{0.82}S$	45.1
	15 t	–	–	–	–	–	$Fe_{0.811}S$	44.8

Note: (1) For *Cobaltine, the average composition determined for six analysis points $(Co_{0.534}Fe_{0.265}Ni_{0.201})As_{1.21}S_{1.18}$ is provided, (2) **Goethite (Gt) or its polymorphic form, with the composition of $Fe_{0.87}Si_{0.02}OOH$ (t6), $Fe_{0.88}Si_{0.03}OOH$ (t8), and $Fe_{1.0}Si_{0.02}OOH$ (t9).

methods were obtained using the equipment stored at "Center of Isotope-Geochemical studies" of IGC SB RAS (EPMA, XRF, AES, AAS, fluid-inclusion thermobarometry, organic matter studies), IGM SB RAS (Raman spectroscopy, stable isotopes), «UltraMicroAnalysis» of IL RAS (LA-ICP-MS), "Baikal Center of Nanotechnologies" of INRTU (ICP-MS), and "IGEM-analitika" of IGEM RAS (LA-ICP-MS, Pb isotope composition).

5. Results

5.1. Mineralogy and petrography of ores and host rocks

The mineralization-hosting metasedimentary rocks are composed of quartz (~30–35%), sericite (~20–25%), carbonates (10%), albite (5%), orthoclase (5%), microcline (5%), muscovite (3%), illite (3%) and chlorite (3%). The accessory minerals are zircon, apatite, tourmaline,

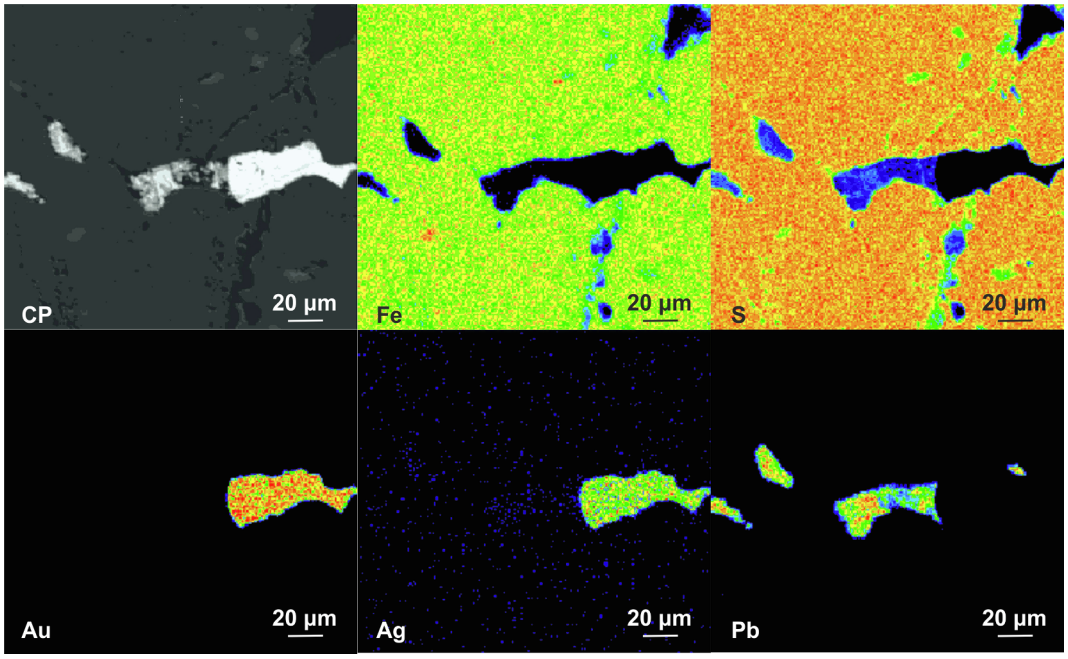

Fig. 10. Gold and galena inclusions through fracture in pyrite-III. Distribution of X-ray radiation intensity of the elements by EPMA.

Table 4
Composition of native gold in pyrite-III (wt. %) from EPMA-data.

Tie-up	Ag	Au	Total
1	12.59	87.41	100.00
2	13.41	86.59	100.00
3	13.95	86.06	100.00
4	10.73	89.27	100.00
5	12.11	87.89	100.00
6	12.49	87.51	100.00
7	11.36	88.64	100.00

titanite, rutile and epidote. The carbonate minerals include (1) early and seldom small inclusion-free rhombic crystals of dolomite and calcite, and (2) large porphyroblasts of siderite replacing earlier carbonates and sandstone cement (Fig. 5a). The siderite porphyroblasts apparently overgrow the schistosity (Fig. 5b) and have inclusions of carbonaceous matter, quartz and other minerals.

The syn-ore alterations of host rocks result in: (1) widespread impregnation of crystalline pyrite, commonly with a rim of quartz, (2) lenticular aggregates of quartz grains produced by regeneration, dissolution and re-deposition of quartz with inclusions of carbonaceous matter and accessory minerals, (3) differently oriented veins and thin winding veinlets of quartz-carbonate composition, (4) lenticular and nest-like clusters of carbonate-bearing pyrite and pectinate quartz over the rims, and (5) veinlet-like sulphide-quartz segregates.

The sulphide mineralization occurs as bands or is disseminated in metasandstones and metasiltstones on the contact with carbonaceous-clayey schists. The rare small carbonate-sulphide veins and veinlets develop through cracks and chaotically cut schistosity. Towards the ore zone, the mineral composition becomes complicated, with appearance of arsenopyrite, galena, tennantite, tetrahedrite, gersdorffite and native gold. The major ore mineral is pyrite, whereas pyrrhotite, chalcopyrite, arsenopyrite, galena, sphalerite, tennantite, tetrahedrite, gersdorffite and alloclasite are present in minor amounts. The hypergenic minerals are goethite and hydrogoethite. Gold primarily occurs as inclusions in sulfide aggregates or in cracks.

Pyrite resembles four distinct generations, including framboidal pyrite-I, thin and dispersed cubic pyrite-II, large megaggregates of pyrite-III, and large crystalline pyrite-IV. Similar observations were made for pyrite in the ores of Sukhoi Log deposits (Large et al, 2007; Meffre et al., 2008; Tauson et al., 2009). The framboidal pyrite-I is the earliest generation occurring as separate grains up to 10 μm, uniformly disseminated in silty sandstones (Fig. 6a). The relics of framboidal pyrite-I are frequently found within small idiomorphic crystals of pyrite-II. The idiomorphic pyrite-II is present as fine-grained dispersed mineralization (Fig. 6b). Pyrite-I and pyrite-II bear largely dispersed submicroscopic-sized Au uniformly distributed through the grains (Fig. 7d; Table 1, for the full dataset see Electronic Supplementary Table 1, Table 2). Later, large meta-aggregates of pyrite-III have associated quartz fringes or strain shadows and are considerably brecciated, with the cracks filled with chalcopyrite, pyrrhotite, galena, sphalerite, gold, tennantite (Fig. 6c-e), and rarer rare-earth element (trace elements) phases (Fig. 8). Large idiomorphic meta-grains of pyrite-III overgrows thin- and fine-grained aggregates of pyrite-II, which captured rutile, quartz and tourmaline. Well-preserved, large cubic crystals of pyrite-IV lacking any signs of deformation and inclusions of other sulfide minerals are observed in quartz-carbonate zones and mark the final stage of mineralization (Fig. 6f).

The ores typically have abundant arsenic minerals, e.g., gersdorffite and two distinct generations of arsenopyrite. High-As arsenopyrite-I (35.1–36.3 at. %) is present as fine (10–30 μm) hypidiomorphic, thin rhombic or acicular crystals regularly distributed in the host rocks (Fig. 9a; Table 3). Arsenopyrite-II with lower As (33.3–33.9 at. %) content is associated with quartz. In sulfide aggregates, arsenopyrite-II was found as large angular or elongated grains within cracks or as an interstitial phase. In some cases, arsenopyrite-II coexists with chalcopyrite, rarer sphalerite, or together with gersdorffite (Fig. 9c). Separate gersdorffite may present as large angular fragments confined to cracks or interstices in pyrite, merged aggregates of arsenopyrite, and as thin elongated grains in the host schists (Fig. 9).

Two distinct generations of pyrrhotite are present. Pyrrhotite-I occurs as fine (0.01–0.05 mm) rounded grains in the host rocks or is captured by pyrite-III meta-aggregates (Fig. 6d). Pyrrhotite-II is present as irregularly shaped coarse-grained aggregates at the edges and within cracks of pyrite-III meta-aggregates, and is closely associated with chalcopyrite (Fig. 6d). The morphology of pyrrhotite-II inclusions follows the shape of cracks and interstices in pyrite-III. Pyrrhotite-I and pyrrhotite-II are distinguished (Table 3).

Table 5
Major oxide contents and trace-element composition (the averages and corresponding ranges) in the host black schists and ores of the Krasniy deposit.

	au $_3$ (71)	OB-1 (117)	au $_2{}^2$ (112)	OB-2(129)	au $_1{}^2$ (81)	au $_1{}^1$ (56)	BS (253)
SiO_2	76.7	69.5	69.4	66.4	68.6	66.2	65.5
	67.3 – 86.9	61.3 – 84.6	61.5 – 86.6	59.9 – 87.9	62.3 – 86.4	57.6 – 75.4	58.9 – 77.9
Al_2O_3	10.3	9.3	15.6	10.5	14.5	15.8	14.6
	8.1 – 21.2	8.6 – 14.7	10.6 – 19.8	9.4 – 16.3	10.6 – 17.2	9.8 – 18.4	10.3 – 21.5
CaO	0.31	0.85	0.37	0.79	0.41	0.7	0.8
	0.2 – 0.5	0.3 – 3.1	0.2 – 0.9	0.3 – 2.6	0.2 – 1.6	0.3 – 2.1	0.3 – 2.81
MgO	0.86	0.94	1.12	1.03	1.08	1.8	1.9
	0.1 – 1.8	0.1 – 2.7	0.3 – 4.1	0.6 – 3.1	0.1 – 3.6	0.1 – 2.8	0.07 – 3.9
Fe_2O_3	4.44	9.84	4.73	8.44	4.91	5.17	5.4
	0.8 – 6.9	3.1 – 16.2	3.2 – 6.1	4.3 – 14.8	2.8 – 6.4	1.8 – 7.4	0.7 – 12.4
K_2O	2.1	1.9	2.0	2.1	2.1	2.8	2.9
	0.5 – 3.4	1.3 – 2.9	1.2 – 3.1	1.7 – 2.9	0.7 – 3.3	1.4 – 3.5	1.6 – 3.6
Na_2O	0.39	0.32	0.39	0.26	0.37	0.42	0.48
	0.2 – 1.7	0.2 – 0.5	0.2 – 0.6	0.2 – 0.5	0.2 – 0.8	0.2 – 1.4	0.4 – 1.9
P_2O_5	0.09	0.23	0.14	0.19	0.12	0.14	0.14
	0.03 – 0.18	0.06 – 0.51	0.03 – 0.21	0.03 – 0.54	0.03 – 0.19	0.03 – 0.24	0.03 – 0.28
MnO	0.05	0.04	0.06	0.05	0.06	0.06	0.07
	0.01 – 0.14	0.02 – 0.11	0.02 – 0.16	0.01 – 0.17	0.02 – 0.12	0.01 – 0.19	0.01 – 0.21
S $_{total}$	0.81	5.67	1.77	3.99	1.81	1.4	1.2
	0.3 – 2.4	1.6 – 9.8	0.7 – 3.4	1.8 – 8.9	0.9 – 3.2	0.5 – 2.8	0.5 – 3.1
CO_2	0.19	1.99	0.37	1.12	0.39	0.41	–
	0.06 – 0.52	0.37 – 9.11	0.21 – 0.57	0.23 – 4.17	0.15 – 0.49	0.09 – 0.87	
LOI	4.82	7.19	6.17	7.81	5.93	6.14	4.74
	2.2 – 6.2	2.7 – 10.7	2.1 – 9.3	3.6 – 11.4	3.1 – 8.1	3.2 – 8.4	2.4 – 7.7
V	56.9	192.8	132.9	282.1	143.4	177.8	164
	29–117	124–467	92–318	169–541	72–296	84–354	97 – 380
Cr	38.9	134.9	103.5	104.6	105.7	106.4	91
	12–68	96–209	63–162	59–223	68–194	51–192	60–186
Co	3.4	16.6	17.5	22.1	16.2	18.2	23.1
	1.1 – 8.7	4.1 – 37.5	2.4 – 37.1	12.9 – 46.7	4.6 – 34.7	3.1 – 40.7	3.4 – 38.9
Ni	20.9	111.7	77.6	178.5	81.4	94.7	55.1
	12.4 – 37.2	42 – 231	31 – 124	137 – 268	34 – 157	19.3 – 144	6.0 – 97
Sr	69.5	78.4	76.3	77.4	78.1	73.5	82.3
	34 – 127	47 – 184	54 – 131	62 – 141	58 – 133	44 – 174	48 – 185
Zn	87.5	203.9	141.6	215.2	126.8	157.2	132.8
	12–153	112–492	57 – 184	106 – 543	31 – 196	37 – 297	17–547
B	257	279.2	281.5	285.4	279.8	276.4	259
	212–298	216–406	206–349	193–437	201–384	176–311	184–437
Cu	57.1	169.3	68.9	171.6	64.2	69.6	63
	42–94	57–501	43–98	62–398	31–121	43–109	30–100
Pb	6.2	33.7	13.9	83.1	19.5	17.9	22.7
	1.8 – 16.3	7.4 – 187.4	2.1 – 27.6	3.1 – 217.2	2.6 – 31.8	2.3 – 34.1	2.1 – 47.6
As	54.9	434.7	104.3	441.6	98.1	97.4	93.5
	14–102	37–519	38–174	48–587	41–198	35–163	31–214
Mo	2.2	9.3	3.6	14.6	3.2	3.1	2.7
	0.5 – 4.3	1.7–42	1.4 – 5.3	1.9 – 50.0	0.6 – 5.8	0.5 – 5.2	0.5 – 25.4
U	1.58	3.72	3.12	8.73	3.43	3.68	3.52
	1.1 – 1.9	1.4 – 6.8	1.5 – 4.7	0.9 – 11.2	1.3 – 5.1	1.3 – 5.4	0.5 – 24.7

Note: Numbers of the averaged values is given in the corresponding column headers; dashes mark contents below detection limits. OB-1 – upper ore body, OB-2 – lower ore body; $au_1{}^1$, $au_1{}^2$, $au_2{}^2$, au_3 – host black shale of the Aunakit formation within the ore body; BS – unspecified rocks of the Aunakit formation picked at a distance from the deposit.

Sphalerite was identified as oval-shaped veinlets in fissures and cavities in pyrite, in interstices of sulfide aggregates, and often forms large irregularly shaped grains near the edges of pyrite aggregates. It has systematically high Cd and Fe content (Table 3). Sphalerite is typically found in the association with chalcopyrite, or may present as separate large loop-like aggregates up to 1 mm in size. Notably, the association of chalcopyrite and sphalerite typically replace pyrite-I, II, III. Fahl ores are observed as aggregates of tennatite and tetrahedrite filling cracks, cavities or intergranular space in pyrite-III, with the rare rims developed after chalcopyrite. Galena was identified within rare thin cracks in pyrite as well as together with native gold (Fig. 10).

The detailed research of some grains of pyrite-I (30 grains) and pyrite-II (59 grains) in 9 samples identified a uniform distribution of gold. This might indicate the finely dispersed or structural forms of gold in pyrite-II with quite a constant content of element from <0.4 to $\sim$1.2 ppm Au (Table 2).

Gold detected in the cracks of pyrite-III either occurs as independent grains or associated with galena (Fig. 10). Some of them are quite large (about 100 μm) and elongated in shape. The morphology of native gold is mainly defined by the crack size. The composition of native gold is rather homogeneous and averages 860–870 in fineness (Table 4).

5.2. Geochemistry of ores and host rocks

Major and trace element contents were measured in over 800 samples collected both from the drill cores within the deposit and host-rock outcrops beyond. The corresponding dataset is provided in Table 5. The black shales enclosing ore mineralization (interbedded sequences $au_1{}^2$ and $au_2{}^2$) are similar in terms of major components and trace elements, irrespective of presence of the ore mineralization and Au content. A few exceptions (CaO, MgO, SiO_2) highlight the difference between lower silt shale ($au_1{}^1$) and black shale sequences ($au_1{}^2$ and $au_2{}^2$) (Table 5). The CaO and MgO content is lower in the upper part of the cross-section compared to the lower one, that agrees with the

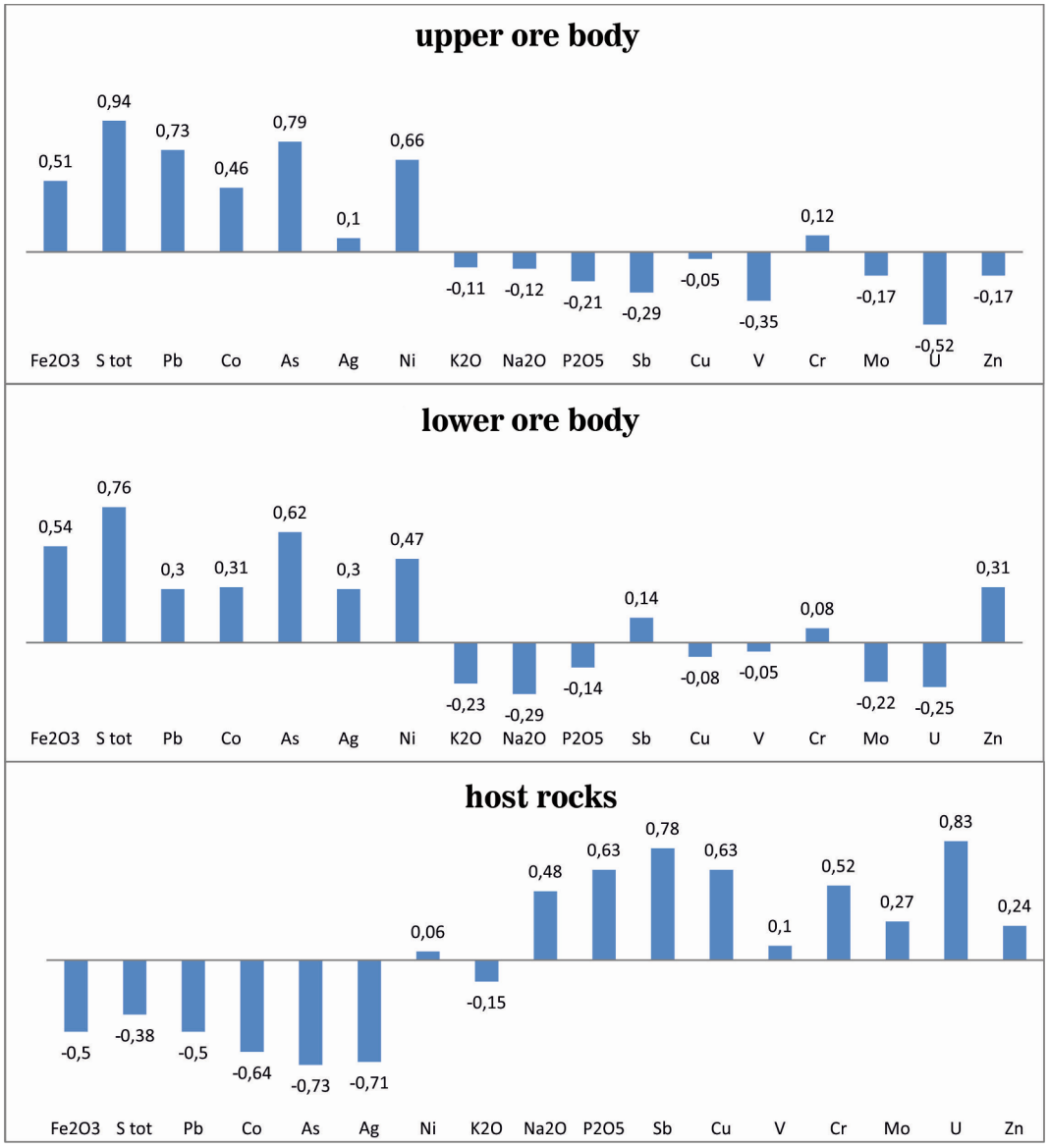

Fig. 11. Correlation diagram for selected major and trace elements with gold content in the ores and host rocks of the Krasniy deposit.

known fact of decreasing proportion of carbonates in the rocks of the Zhuya group versus Dal'naya-Taiga group (Chugaev et al., 2018). An increase in SiO_2 content is marked in the upper part (au_3), which is also common for the overlying sediments of the Vacha Fm, with the maximum silica content in sediments of the Zhuya stage (~80%). In the samples with notable gold content, the Fe_2O_3 and S contents increase twice at less notable increase of CO_2, P_2O_5, CaO (Table 5). Variations of alkalis (Na, K, Li, Rb and Cs) from the ore zones relative to ore-barren sediments are negligible.

The black shales sampled within the deposit (au_1^2 and au_2^2; Table 5) and far beyond the ore bodies (Fig. 11; Table 5) have similar trace elements patterns. However, the samples from the ore bodies display an increase of Ni, Cu, Pb, As, Mo, U, Zn and V contents. The top and bottom of the section show similar elemental correlations of the two types. The first one includes major oxides (Al_2O_3, TiO_2, K_2O, Na_2O and P_2O_5 and trace elements V, Sb, Cu, Cr, Zn, Mo, U, Be with pair correlation between all correlation from 0.3 to 0.8 (more than 70 samples). The second group is composed of Fe_2O_3, Pb, Co, Ni, Ag, As, which show a significant correlation with gold. In the cases of barren sediments, gold highly correlates with U (CC +0.8), to a lesser extent Sb, Cu, Cr and P_2O_5 (CC ~ +0.5), Mo and Zn (CC ~ +0.25), which is destroyed at the stage of ore zones formation. U, P_2O_5, V and Mo show high positive intercorrelations (CC > +0.6) irrespective of sampling site as all these elements enrich mainly in the organic matter.

5.3. Phase and chemical composition of carbonaceous substance

Within the deposit, the organic carbon (Corg) contents in the Aunakit Fm rocks vary from 0.64 to 3.59 wt%. Irrespective of the sampling site location, the correlation coefficient (CC) between the contents of gold and carbon is −0.104 over the entire selection (168 samples) (Fig. 12; Electronic Supplementary Table 2). At that, CCs of the upper and lower ore bodies (+0.09 in 84 samples) and (−0.06 in 28 samples), respectively, do not differ much from CCs of host rock samples at the edge of deposit, e.g. −0.14 in 56 samples for the 95% level of significance regarding the Student's criterion. Remarkably, the sediments of the overlapping Vacha series are distinguished by maximum (6.82%) organic substance content available in the rock. The lack of correlation between gold and organic carbon content indicates that gold content and precipitation was unlikely controlled by redox sorption from an external fluid.

The bitumen content in the samples of the Aunakit Fm beyond the

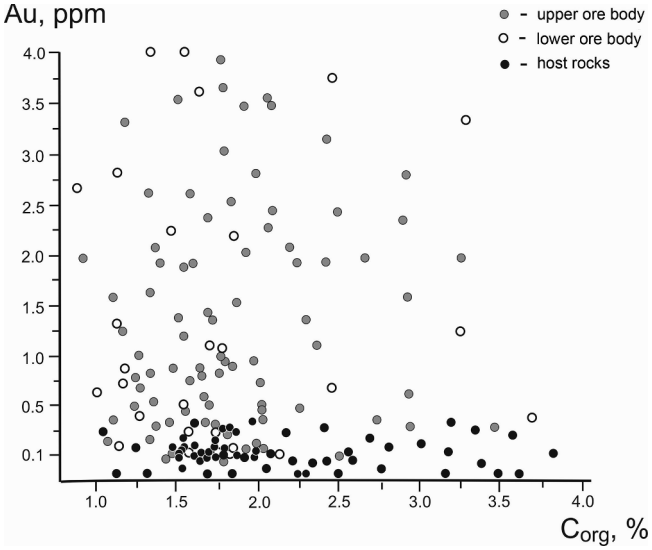

Fig. 12. Relationship between bulk Au and organic carbon contents in the ores and host rocks.

deposit ranged from 0.007 to 0.011%, whereas for the Vacha Fm, corresponding values are up to 0.013%. When approaching the ore zone, the amount of bitumen is five times higher (0.041–0.049%). In the Aunakit Fm, the Au concentrations measured in bitumens vary from 0.91 to 1.25 ppm, which are close to those obtained for Sukhoi Log (Razvozzhaeva, 2015). Moreover, in the Vacha Fm, the Au abundance in bitumens is systematically below detection limits irrespective to proximity to the ore bodies (Table 6). No correlation was observed between the Au contents in the bulk samples and in recovered bitumens.

The IR spectra of organic substance display the absorption bands of complex (1720–1740 cm^{-1}) and simple ether (1000–1150, 1280 cm^{-1}), as well as aliphatic compounds (1380–1390, 1460–1470, 2800–3000 cm^{-1}) (Fig. 13). The presence of aromatic structures in bitumoids of the Bodaibo synclinorium deposits is indicated by the absorption shoulder near 1600 cm^{-1} within the intense band of C═O (1740 cm^{-1}). The band in the 3200–3400 cm^{-1} area indicates the presence of OH-groups related to carbonate acids and alcohols. Similar absorption shoulder were obtained for bitumens from the Sukhoi Log deposit (Razvozzhaeva, 2015)

The element composition of alcohol-benzene bitumoids (ABB) extracted from the metasediments typically has C (63.9%), H (9.4%), N + S + O (total of 27.2%), that is close to the corresponding values for bitumens from the Sukhoi Log and Goletz Vysochaishyi deposits (C 63.8–64.9%; H 7.2–7.6%, N + S + O 22.7–27.9%) (Budyak et al., 2015a). The highest content of metals of organophile geochemical affinity (Table 7) is commonly higher in the fractions enriched with functional groups (asphaltene acids – AA, asphaltene – As) (Razvozzhaeva et al., 2011; Sugiyama, 2015). To summarize, the phase and chemical composition of the carbonaceous substance studied here resembles that reported earlier for the host rocks of the Sukhoi Log ore deposit.

5.4. C and S isotope composition

The isotope composition of bulk carbon (in $\delta^{13}C$ notation) of host rocks, hydrothermally-altered zones and ores varies within a narrow range from −17.3 to −19.1‰, and is similar in the two ore bodies and samples of the host sediments (Table 8). The carbon isotope composition of the dissolved carbonaceous substance (DCS) and kerogen (undissolved carbonaceous substance, UCS) show insignificant variations (-28.5‰ and −21.9‰, respectively) (Table 8).

The isotope composition of sulfur (in $\delta^{34}S$ notation) of pyrite-III ranges from −4.5 to −6.9‰ (Table 8), and corresponds to that of sulfur from pyrite-II hosted by the Aunakit Fm rocks (from −5.2 to −6.6‰; Table 8). There is an apparent trend of $\delta^{34}S$ decrease within the overlying sediments of the Vacha formation (down to −7.4‰), that agrees with the results obtained earlier for unaltered rocks sampled away from the deposit (Chugaev et al., 2018).

5.5. Pb isotope composition of sulfides

The contents of Pb, Th and U in pyrites from ore zones and barren rocks range widely (11–1652 ppm of Pb, 0.16–7.9 ppm of Th, 0.15–4.8 ppm of U) (Fig. 14, Table 9). Pyrite from barren rocks has

Table 6
Organic carbon and gold contents in carbonaceous schists and bitumen from the Krasniy deposit as compared to corresponding values for the Sukhoi Log deposit.

Formation	Deposit, position	C_{org}, % CB + ABB, %	Au in native rocks, ppm	Au in CB, ppm	$\delta^{13}C$ в CB, ‰	$\delta^{13}C$ in IOS
vc	Krasniy, Lozhok syncline	4.19 0.015	0.002	n.d.	−28.2	−21.3.
vc	Krasniy, Eastern zone	4.82 0,013	0,002	n.d.	−27.9	−21.1
au_2^2	Krasniy, supra-ore zone	1.71 0,041	0.1	1.25	−28.7	−21.1
	Krasniy, ore zone	3.09 0, 47	> 1.0	0.97	−28.0	−20.8
au_2^2	Krasniy, flank	2.67 0,007	0.015	1.16	−27.7	−20.7
au_2^2	Krasniy, beyond ore field	1.46 0,011	0.005	0.91	−28.8	−21.2
hm	Sukhoi Log, near-ore zone	0.65 0,037	1.10	1.55	−27.1	−17.5
hm	Sukhoi Log	0.83 0.041	1.00	0.91	−27.2	−17.6
hm	Sukhoi Log (Western quarry)	0.93 0.024	0.30	1.38	−27.4	−17.8
hm		0.70 0.013	0.60	1.61	−26.8	−17.2
hm	Sukhoi Log, beyond ore field	1.66 0.011	0.02	0.99	−26.9	−17.3

Note: the data for the Khomolkho formation were borrowed from Budyak et al. (2015a,b).

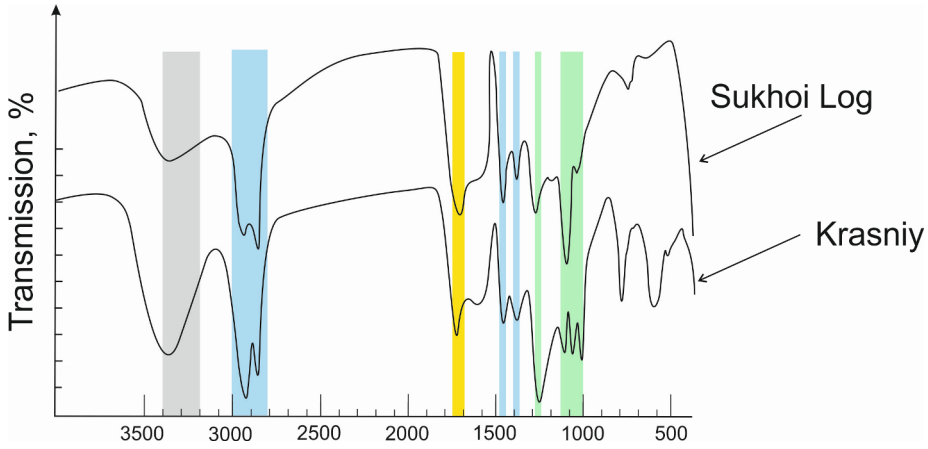

Fig.13. IR spectra of bitumens extracted from host black schists of the Sukhoi Log and Krasniy deposits.

Table 7
Concentration of selected trace and ore elements in the alcohol-benzene and chloroform bitumens of the Krasniy deposit.

	Bitumoid fraction	Mass %	Cu, ppm	Zn, ppm	Ni, ppm	U, ppm	Au, ppm
Ore zone	Asphaltene	2.4	134.4	480.1	21.7	127.7	58.3
	Asphaltene acids	5.3	148.0	218.2	37.6	2.28	1.81
	ABB	17.8	15.2	14.1	1.4	2.94	0.54
	BR	21.7	1.34	3.19	0.21	21.1	0.31
	CS	53.1	0.11	0.46	0.02	0.29	0.23
	CB + ABB	100	14.12	26.53	2.81	7.81	1.39
Deposit flanks	Asphaltene	1.7	209.4	374.5	38.6	158.4	46.7
	Asphaltene acids	6.2	127.3	220.5	21.4	6.75	2.67
	ABR	19.2	21.5	33.28	4.51	2.41	0.61
	BR	26.4	1.78	3.35	0.24	9.11	0.43
	CS	46.5	0.48	2.73	4.81	0.69	0.27
	CB + ABB	100	16.27	28.58	5.14	6.29	1.27

Note: Determined with atomic absorption by Vall G.A. (VSNIIMS); ABR – alcohol benzene resins, BR – benzene resins, CS – carbonaceous substance.

Table 8
Bulk carbon and pyrite (II, III) sulfur isotope composition of the hosting rocks and ores at the Krasniy deposit.

Sample code	Formation/ore body	$\delta^{13}C$, ‰	$\delta^{34}S$, ‰
KR-59	Vc	−19.0	− 7.4
KR-60		−18.3	− 6.8
K-16		n.d.	− 6.9
KR-1	Au_3	−17.8	− 5.7
KR-2		−18.9	− 6.4
KR-3		−19.1	− 6.2
K-171	OB-1 (au_3)	n.d.	− 5.1
KR-4		−18.3	− 5.7
KR-5		−19.0	− 4.7
KR-6		−18.7	− 4.7
KR-9		−17.3	− 6.9
KR-10	Au_2^2	−19.0	− 6.3
KR-12		−18.1	− 6.6
KR-19		−19.0	− 5,2
K-206	OB-2 (au_2^1)	n.d.	− 4.5
KR-23		−19.1	− 6.5
KR-26		−18.4	− 4.7
KR-39	Au_1^2	−19.1	− 6,4
K-108		n.d.	− 5.3
K-141		n.d.	− 5.6

Note: OB-1 – upper ore body, OB-2 – lower ore body.

more reproducible contents of Pb (35–202 ppm) against pyrite from auriferous ores (11–1652 ppm). The measured values of Pb isotope ratios lie within the ranges of $^{206}Pb/^{204}Pb$ = 18.40–18.89, $^{207}Pb/^{204}Pb$ = 15.65–15.70 and $^{208}Pb/^{204}Pb$ = 38.15–38.93. The observed heterogeneity of $^{238}U/^{204}Pb$ (0.05–4.1) and $^{232}Th/^{204}Pb$ (0.01–7.2) ratios suggest the presence of variable radiogenic addition of ^{206}Pb, ^{207}Pb and ^{208}Pb due to radioactive decay of ^{238}U, ^{235}U and ^{232}Th. To account for it, the acquired values of Pb isotope ratios were corrected for the supposed age of ore-forming processes in the Bodaibo region (450 Ma; Laverov et al., 2007). The corrected values of isotope ratios $(^{206}Pb/^{204}Pb)_t$, $(^{207}Pb/^{204}Pb)_t$ and $(^{208}Pb/^{204}Pb)_t$ show a smaller scatter of 18.33–18.65, 15.65–15.68 and 38.13–38.82, respectively. However, the variations remain quite significant and exceed the analytical error. The calculated values of variation coefficient (*V*, %) amount to 0.46% ($^{206}Pb/^{204}Pb$), 0.07% ($^{207}Pb/^{204}Pb$) and 0.46% ($^{208}Pb/^{204}Pb$). Pyrite from the gold mineralization is similar to the pyrite from barren rocks both in the calculated ranges of Pb isotope composition and in the values of *V* parameter. The same ranges include the results of individual Pb analyses of pyrite and galena samples obtained earlier at the Krasniy deposit (Chugaev and Chernyshev, 2017).

5.6. Fluid inclusion composition

For fluid inclusion analysis, twenty quartz plates were made from quartz-sulfide aggregates that belong to the upper and lower ore bodies. The studied quartz samples primarily contain two-phase liquid + gas (L + G) inclusions 30–100 μm in size, with minor amount of purely gaseous (G) inclusions. Based on the morphology and location, the inclusions are regarded to as primary and secondary. For detailed examination, only primary two-phase fluid inclusions 50 μm or more in size were picked (Fig. 15). The size of the gas bubble varies considerably, often from 20 to 60% vacuole volume, some finer inclusions contain bubbles, which occupy nearly entire vacuole volumes. The

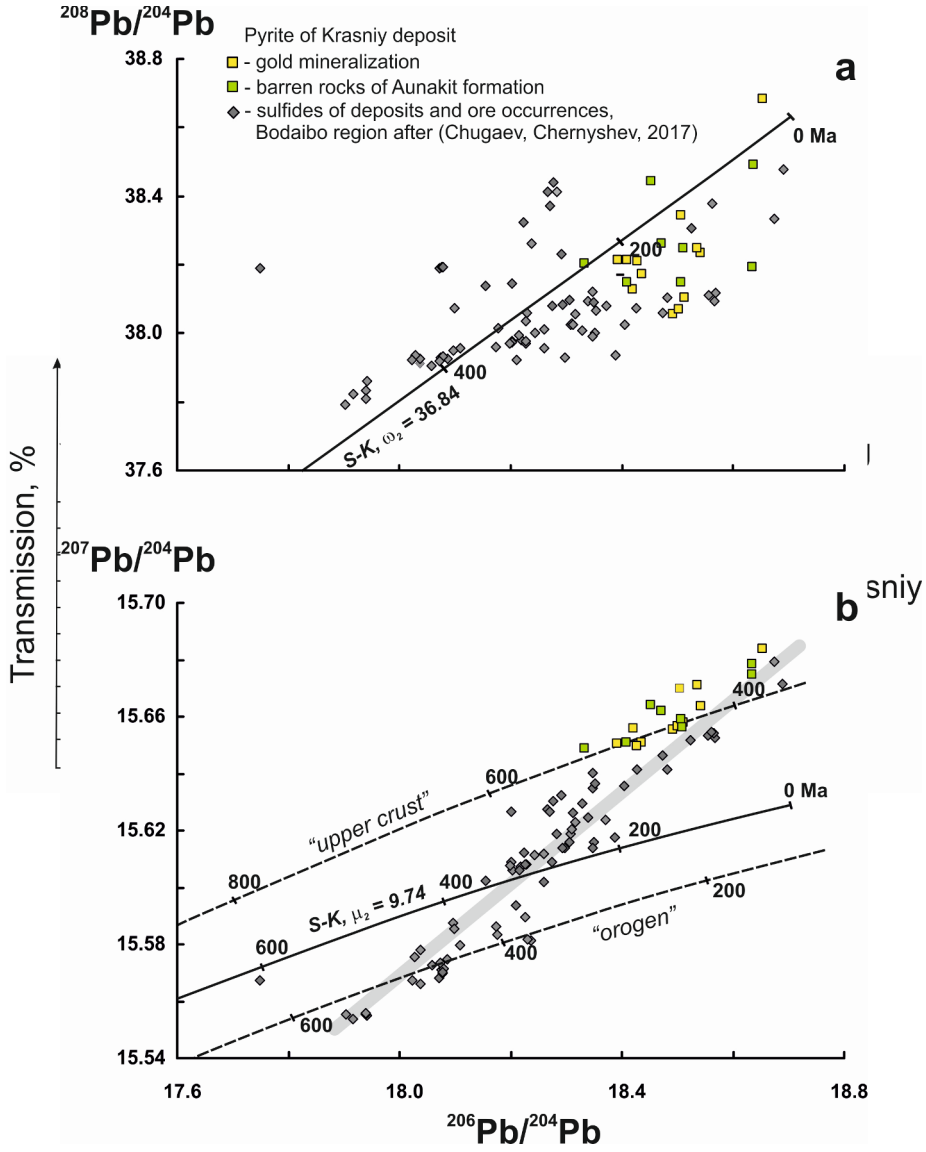

Fig. 14. Pb isotope composition of sulfides from the ore intervals at the Krasniy deposit as compared to those from the Sukhoi Log and Verninsky gold deposits.

average temperature of ice melting reached from −5.5 to −6.4 °C. The average temperature of dioxide melting reached −61.4 °C, which is lower than the melting temperature of carbon dioxide, and indicates the presence of nitrogen or methane. At temperatures below + 3.0 °C, all inclusions display clathrates of carbonate composition. A denser rim around the bubble indicates the carbon dioxide presence in the system (Fig. 15a, b).

Primary two-phase inclusions homogenize into a liquid phase at temperatures of 270–320 °C. There is some minor spread in the temperatures of homogenization both in quartz from the upper (270–300 °C) and lower (300–320 °C) ore zones. The average temperature of fluid inclusion eutectics for the former is −29 °C, and −34 °C for the latter. The salinity of a liquid phase in inclusions for the upper ore zone varies within 3.2–3.8 wt% $NaCl_{equiv}$, whereas for the lower one, it ranges from 3.6 to 4.5 wt% $NaCl_{equiv}$. The fluid density calculated with the FLINCOR software for both ore zones is about 0.8 g/cm^3 and 1.1 g/cm^3, respectively. The estimated pressure was about 0.5 kbar (Table 10).

Based on the Raman spectroscopy data, a gaseous phase of inclusions is mostly composed of CO_2 (64.7–92.1 mol. %), with minor N_2 and CH_4 (2.14–19.6 and 2.97–15.7 mol. %, respectively) (Table 11, Fig. 16). Some inclusions show presence of H_2S (Fig. 16).

6. Discussion

6.1. Conditions and mechanisms of multi-stage ore formation

When equilibrated with pyrite and pyrrhotite at low pressures ~1 kb, sphalerite must contain 19–20 mol. % FeS (Scott and Barnes, 1971). Sphalerite from the ore bodies has a markedly lower FeS content (Table 3), which indicates the overprinting nature of sphalerite crystallization relative to the association of pyrite-II + pyrrhotite-I. Sphalerite is also in a clear disequilibrium with arsenopyrite, as in a triple association (sphalerite-pyrite-arsenopyrite) sphalerite must contain >10 mol. % FeS (Scott, 1983). Instead, high Cd contents are commonly specific to low-T sphalerite (Tauson and Chernyshev, 1981). In all samples, arsenopyrite with high As content can neither exist with pyrite + pyrrhotite association nor with pyrite only, as it must contain less than 33 at. % As (Scott, 1983; Barton and Skinner, 1979). The presence of two pyrrhotite generations in the association with pyrite also points to the disequilibrium within these associations, as a simultaneous hydrothermal crystallization of pyrite + pyrrhotite, pyrrhotite should have more Fe-rich composition than that measured for pyrrhotite-I in the Krasniy deposit ores. Additionally, if the crystallization of arsenopyrite, pyrite-II and pyrrhotite-I proceeded

Table 9
Pb isotope composition (measured values) of pyrite from the Krasniy deposit.

№	Sample number	Pb, mkg/g	Th, mkg/g	U, mkg/g	$^{206}Pb/^{204}Pb$	$^{207}Pb/^{204}Pb$	$^{208}Pb/^{204}Pb$	μ_2	ω_2	Тм
Pyrite in the gold ore mineralization										
Northern ore body										
1	Kr-13	42	4.6	1.3	18.6672	15.6789	38.6320	9.96	38.3	235
2	Kr −35	35	1.5	1.6	18.8939	15.6973	38.9265	9.99	39.5	154
Lower ore body										
3	Kr −71	69	0.18	0.51	18.5807	15.6660	38.3446	9.93	37.2	196
4	Kr −72	941	0.17	0.84	18.4246	15.6562	38.2150	9.92	37.3	270
5	Kr −92	92	0.16	0.31	18.5534	15.6722	38.3593	9.96	37.5	215
6	Kr −100	261	2.5	0.57	18.4035	15.6512	38.3289	9.91	37.9	280
Upper ore body										
7	Kr −108	11	1.2	0.15	18.5622	15.6595	38.2917	9.90	36.3	216
8	Kr −142	123	1.1	0.57	18.5356	15.6591	38.2011	9.91	36.5	206
9	Kr −155	29	2.2	0.69	18.5599	15.6578	38.3817	9.90	37.3	248
10	Kr −156	28	1.7	0.70	18.5569	15.6569	38.4019	9.89	37.6	252
11	Kr −203	23	2.1	0.41	18.5015	15.6559	38.4492	9.90	37.8	268
12	Kp-205	1652	0.88	1.1	18.5049	15.6569	38.1498	9.91	36.4	212
Pyrite in the barren host rocks										
Northern ore body										
13	Kr −17	202	2.5	0.48	18.6468	15.6754	38.3105	9.95	36.5	150
14	Kr −31	64	1.5	0.85	18.7049	15.6823	38.6760	9.97	38.4	155
15	Kr −45	114	1.8	0.62	18.5343	15.6607	38.2620	9.91	36.8	212
Lower ore body										
16	Kr −82	41	0.65	0.39	18.5212	15.6649	38.3965	9.94	37.8	244
17	Kr −84	83	0.98	0.83	18.5053	15.6670	38.6023	9.95	39.2	262
Upper ore body										
18	Kr −127	43	1.2	0.38	18.5554	15.6587	38.3975	9.90	37.4	203
19	Kr −188	85	7.9	4.8	18.6270	15.6653	38.4428	9.91	38.3	320
20	Kr −200	35	1.6	0.98	18.5538	15.6592	38.3084	9.90	37.4	268

Note. The total error of their analysis was within 0.03% (±2SD). The μ_2, ω_2 and Тм model parameters were calculated with correction to measured Pb ratios for the supposed age of ore mineralization (450 Ma).

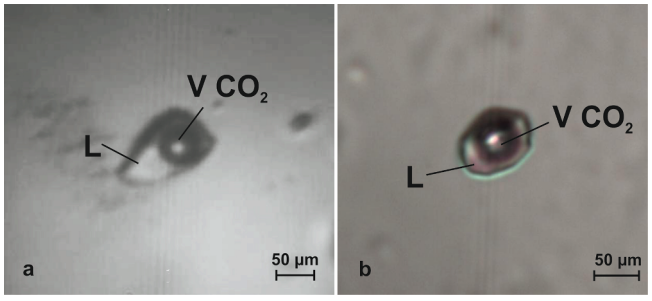

Fig. 15. Microphotographs of fluid inclusions in quartz from the upper (a) and lower (b) ore bodies.

simultaneously, based on the phase diagram of Fe-As-S system, the pyrite-pyrrhotite transition proceeds at T ~ 400–491 °C and sulfur fugacity ($lgfS_2$) between −7.5 and −5.5 bar (Toulmin and Barton, 1964; Kretschmar and Scott, 1976). In the case of lower-Fe pyrrhotite-II, the above association should exist at much higher temperatures, that contradicts the maximum temperature of regional metamorphism within the region (380 °C at pressure 5–6 kb; Petrov and Makrygina, 1975).

Development of pyrrhotite at such low temperatures (< 380 °C) is feasible based on pyrite-I, II in the presence of organic carbon in the rock (Hall, 1986). According to Tomkins (2010) and Damdinov et al. (2019), during the metamorphism of sulfide-bearing rocks in the presence of carbon, this process proceeds through reaction:

$$2H_2O + C + 2FeS_2(\text{pyrite}) \rightarrow CO_2 + 2H_2S + 2FeS\ (\text{pyrrhotite})$$

Beside the pyrrhotite formation, the reaction leads to release of CO_2– and S-bearing metamorphic fluids as well as a number of trace metals originally captured in pyrite, including gold (Large et al., 2011). The following appearance of pyrite-III and low-Fe pyrrhotite-II is caused by the emergence in the S-bearing fluid phase. Experimental data indicate that the trace elements released might lead to their redistribution and crystallization of the overprinting polymetallic association with gold coarsened to the grain size of up to 1–1.5 mm (Kalitkina, 1971).

Overall, the formation of the observed mineral association was likely a multi-stage process with varying thermodynamic conditions (Fig. 17). At the very first stage, framboidal pyrite-I with Ni impurity and uniform distribution of dispersed (nano-sized) Au^0 over the surface was formed in the sedimentary sequence (Tables 1, 2, Fig. 7). Further, with P-T conditions progressively increasing as a response to catagenetic transformations (Yapaskurt, 2005) (P ~ 1–2 kbar, T < 200 °C), the original sulfide association was replaced by fine-grained idiomorphic pyrite-II crystals adsorbing micro-sized native gold on the growing crystal surfaces (Tables 1, 2). Consequently, a relatively high-T association (probably up to ~380 °C) of pyrrhotite-I + arsenopyrite-I was formed. The morphology of pyrrhotite-I close to the shape of pyrite-I implies possible development of pyrrhotite as a pseudomorph after diagenetic pyrite-I. Similar forms of pyrrhotite liberation are identified at the Sukhoi Log deposit (Large et al., 2007). Formation of meta-aggregates of pyrite-III, pyrrhotite-II, native gold (Fig. 10, Table 4) and the overprinting polymetallic association containing Cd-rich sphalerite proceeded synchronously. The same metasomatic process led to replacement of Fe-free diagenetic carbonates (calcite) by ankerite, later siderite, and synchronous development of quartz in rocks and formation of elongated veinlet-vein zones. The post-ore stage is marked by development of large crystals of idiomorphic pyrite-IV in the quartz-carbonate rim.

6.2. *The role of geochemistry of host sedimentary sequences and behavior of major components*

The contents of K_2O, Na_2O and MgO within the ore and barren zones of the deposit do not vary significantly (Fig. 18). Though quartz is the most widespread vein mineral in the ore zone, the total content of SiO_2 in both zones is similar. This points to the absence of SiO_2 supply into the zone of ore deposition from the external sources. Similar conclusions were made earlier for the Sukhoi Log and Golets

Table 10
Results of P-T-X examination of fluid inclusions in quartz from the upper and lower ore bodies of the Krasniy deposit.

	n	T_{hom}, °C	T_{eutect}, °C	Tm ice, °C	Tm CO_2, °C	Th CO_2, °C	Hom. Mode CO_2	Tm cl., °C	Salinity, wt. % $NaCl_{eq}$	Density, g/cm^3	Pressure, bar
Quartz from the upper ore body	75	270–300	− 31 – − 27	− 6.4 – − 5.2	− 62.0 –59.2	−14.2 – 10.7	L	− 4.2 – 3.0	3.2–3.8	0.8	750–370
Quartz from the lower ore body	80	300–320	− 34	− 6.4 – − 5.5	− 62.4 –59.6	−14.9 – 11.3	L	− 4.5– 3.0	3.6–4.5	1.1	890–440

Table 11
Representative composition of fluid inclusions calculated from the Raman spectroscopy data.

Fluid inclusion	Mol. %			
	1	2	3	4
CO_2	92.1	92.6	82.5	64.7
N_2	2.14	4.39	7.14	19.6
CH_4	5.80	2.97	10.4	15.7

Vysochaishy deposits (Nemerov et al., 2010; Budyak and Bryukhanova, 2012). The ore zones display a distinct increase of Fe and S contents due to sulfide mineralization (Fig. 18), increase of CaO, P_2O_5 and CO_2 within the intervals with maximum gold contents related to the appearance of late siderite and monazite associated with pyrite-III (Fig. 8).

Noteworthy, within the Krasniy ore zone, there is no increase of K_2O and Na_2O contents, which show negative correlation with gold. Similar behavior of these elements was identified in bulk samples collected at the Sukhoi Log deposit (Budyak, 2009). This fact contradicts the hypothesis of the syn-ore K-Na metasomatism being the source for ore materials (Rusinov et al., 2008). High correlation of gold with the organophilic elements (Mo, U, S and As) (Fig. 19) in the near-ore space might be the indication of pre-ore process genetically linked with organic fluid. According to Yudovskaya et al. (2011), this specific fluid could be released during catagenetic transformation of the host sedimentary strata in the Ediacarian, coeval to starting deformation and folding of the Bodaibo paleobasin and deposition of the overlying molasses of the Anangrsky Fm (Chugaev et al., 2018). The absence of correlation between gold and C_{org} contents in the ore-rich zones and its apparent affinity of gold with CO_2 (as seen CO_2 predominance in fluid inclusions) (Fig. 16, Table 11) stems from the involvement of a mobile fluid phase rich in carbonic acid. The existing concepts assume that, at the final stage of ore generation, the ore-forming system of the Sukhoi Log-type had a closed nature (Buryak et al., 2002; Nemerov et al., 2010; Dubinina et al., 2014; Meffre et al., 2008; Large et al., 2007). Thus, we suggest that CO_2 in the fluid derived from metamorphism-driven decarbonization of organic substances. Gold mobilization was related to reduction of a metamorphic fluid that is indicated by highly dispersed (nano-sized) Au^0 uniformly distributed over the surface (Tauson et al., 2010), as well as siderite associated with pyrite. Thus, the obtained data point to low mobility and limited redistribution of the ore components including gold *in situ*, and pre-ore concentration of gold in metasediments (Fig. 20).

The content of bulk organic carbon (~99.5% insoluble carbonaceous substance (IOS) and ~0.5% of bitumen in all explored deposits of the Bodaibo region varies within 1.5–4%, with a maximum of 7% in the Sukhoi Log ore zone. Identical compositions of bitumoids in the Krasniy and Sukhoi Log samples indicate similar sources for the organic substance in the metasediments (Fig. 13). As was suggested above, the absence of correlation between gold and bulk C_{org} implies that IOS of the host black shales was not the important factor contributing to sorption of gold from the CO_2-dominated fluid. Instead, the bitumens as relics of the primary dispersed carbonaceous substance of metamorphosed schists inherit the geochemical potential at the pre-catagenic stage (Razvozzhaeva et al., 2011). Sugiyama (2015) showed in experimental work that a crude oil has the capacity to dissolve noble metals in the concentrations of two orders higher than in the ore-forming hydrothermal fluids (Simmons and Brown, 2006). The obtained concentrations of Au in the solved component of organic substance of the Khomolkho and Aunakit Fm (>1 ppm) give the grounds to consider their possibility to transport noble metals in the catagenic fluid at the pre-ore stage of substance redistribution. Several studies revealed also that a capacity of such carbon-rich fluids to dissolve and transfer metals might be increased via nitrogen addition (Buchler, 1978; Manning and Gize, 1993; Fuchs et al., 2015). A significant amount of

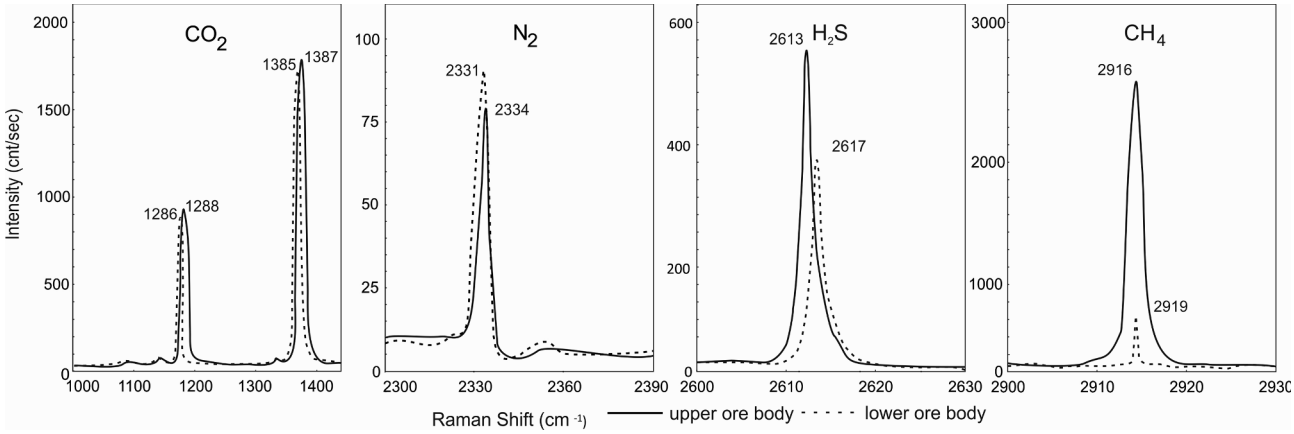

Fig. 16. Representative spectra for CO_2, N_2, CH_4, and H_2S Raman peaks in primary gas–liquid fluid inclusions in quartz from the upper (a) and lower (b) ore bodies of the Krasniy deposit.

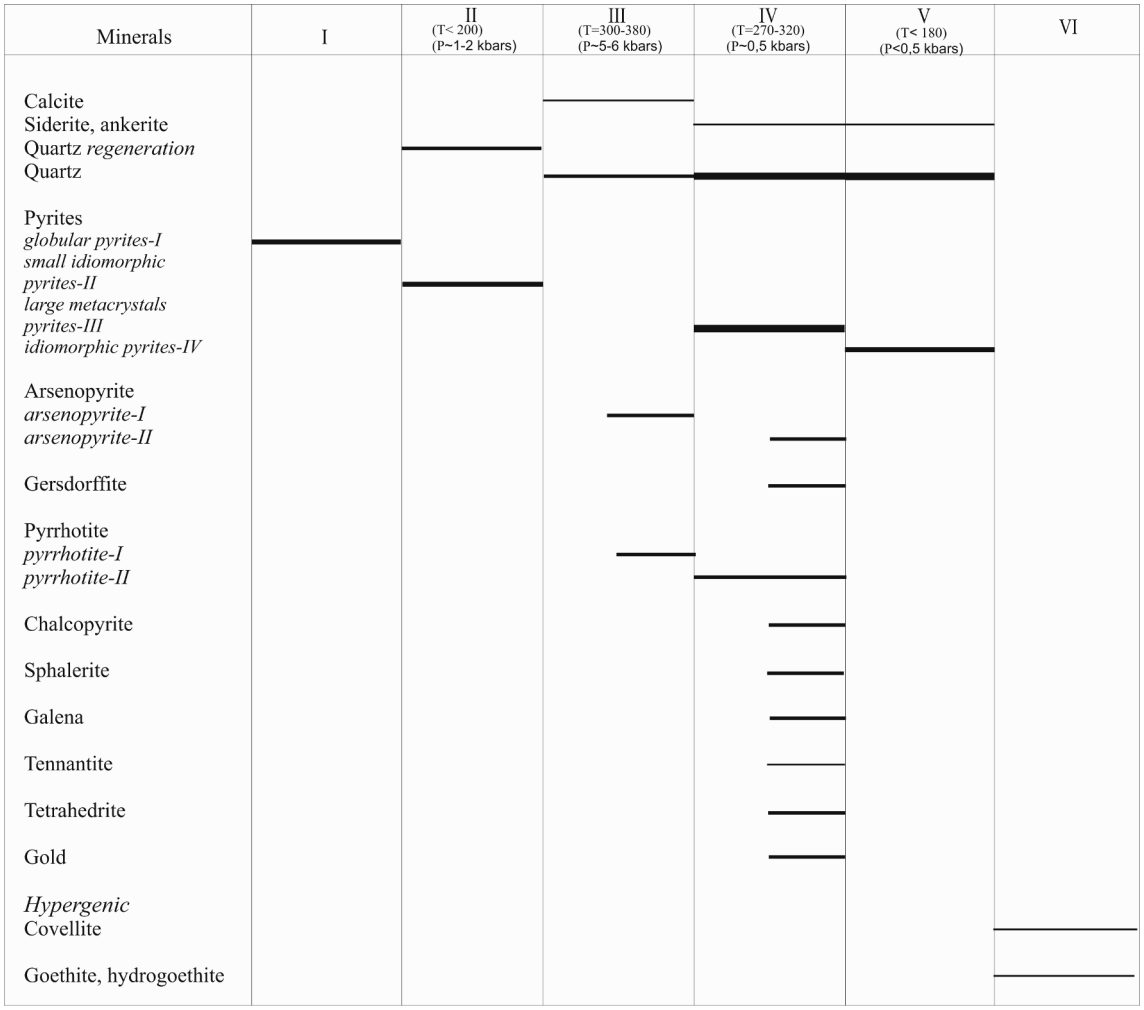

Fig. 17. The formation sequence of multi-stage ore mineralization in the Krasniy deposit.

heavy non-hydrocarbon fractions in the compositions of bitumoids is confirmed by the presence of N + S + O association of elements (Varshalll et al., 1994), as well as abundant nitrogen in the analyzed fluid inclusions in quartz of gold ore bodies at the Krasniy deposit (Fig. 16, Table 11). Therefore, one might suspect that the inheritance of sidero-chalcophyle geochemical affinity with gold for the Aunakit and Khomolkho Fm relates to the sedimentation stage, and destruction of organic substance at the stage of metamorphic transformation caused release of a carbon dioxide fluid involved further in the ore process.

6.3. Isotope characteristics and the source of ores at the Krasniy deposit

Gold-bearing pyrite (pyrite-II, III) is quite homogeneous it terms of $\delta^{34}S$ variations (from −4.7 to −6.9‰, average of −5.7‰ for 20 analyses), and apparently resembles those of the diagenetic pyrite (pyrite-I) (Fig. 21), at similar isotope composition of pyrite within the

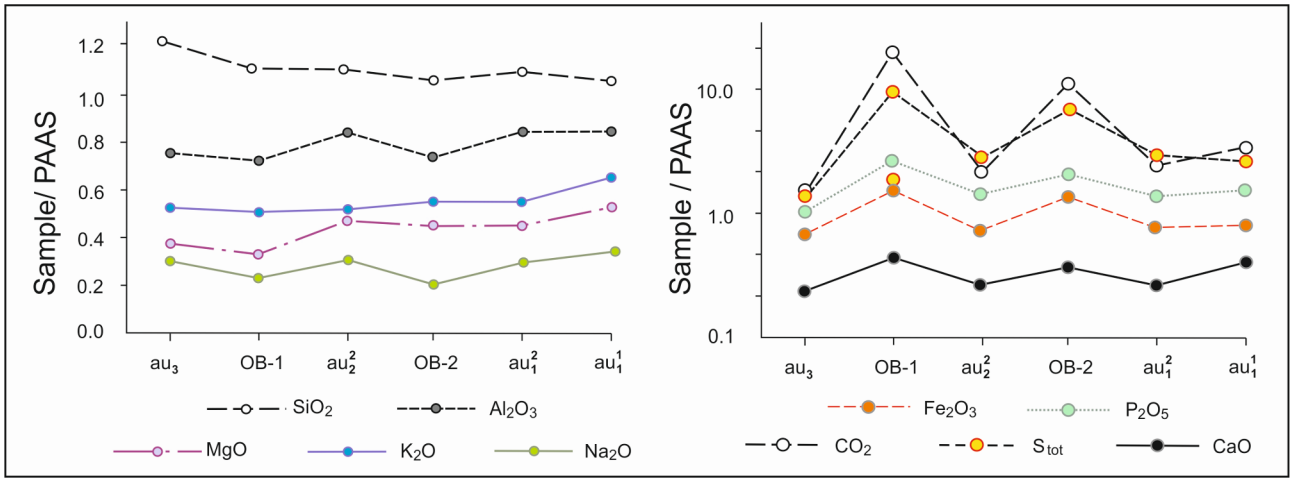

Fig. 18. Major element variations of near-ore rocks and ores of the Krasniy deposit. au_1^1, au_1^2, au_2^2, au_3 – bedded sequences of the Aunakit Fm; OB-1 – upper ore body, OB-2 – lower ore body.

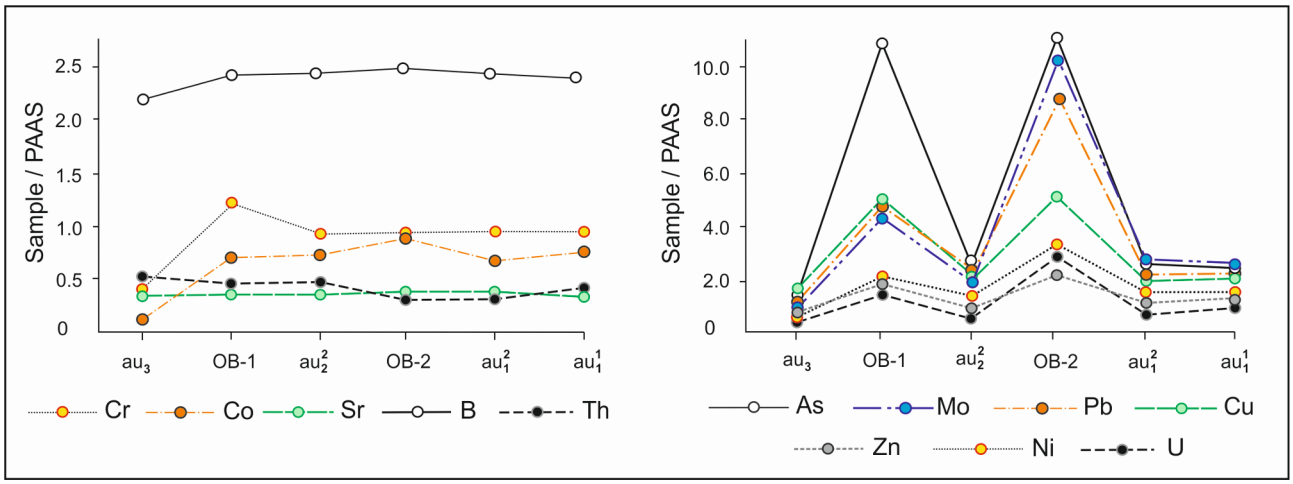

Fig. 19. Trace and ore element variations in the near-ore rocks and ores of the Krasniy deposit. au_1^1, au_1^2, au_2^2, au_3 – bedded sequences of the Aunakit Fm; OB-1 – upper ore body, OB-2 – lower ore body.

ore bodies. However, a certain difference in $\delta^{34}S$ signatures is observed for the deposits hosted by distinct stratigraphic sequences. More specifically, the $\delta^{34}S$ of pyrite from the Khomolkho Fm, which hosts both Sukhoi Log and Golets Vysochaishy deposits (Chugaev et al., 2018) is reflected by a heavier isotope composition, with the average $\delta^{34}S$ value of +3.9‰ (Fig. 21). This evidence agrees with the identified pattern of S isotope composition variations in metamorphic pyrite from the Neoproterozoic sequences of BPP, i.e., a regular lightening of S isotope composition upwards with the minimum value in the Yudoma group metasediments (Dogaldyn Fm, −12.1‰) (Fig. 21). These variations do not follow a general pattern of S isotope evolution in the Neoproterozoic oceans (Chang et al., 2008; Chugaev et al., 2018), but instead reflect the decrease of ^{34}S proportion due to a changing paleotectonic environment of the Bodaibo foreland basin in the Ediacarian (Nemerov et al., 2010; Powerman et al., 2015; Gladkochub et al., 2013; Budyak et al., 2016).

Provided comparison of the ore mineralization from the large deposits reported earlier (Sukhoi Log, Verninsky) and the Krasniy deposit indicates more homogeneous Pb isotope composition in the latter. In particular, this is highlighted by much higher variation coefficient values for $^{206}Pb/^{204}Pb$ and $^{207}Pb/^{204}Pb$ isotope ratios in the Sukhoi Log and Verninsky deposits ($V_{6/4}$ = 0.7–0.9%, $V_{7/4}$ = 0.13–0.17%) (Chernyshev et al., 2009; Chugaev et al., 2014). The Pb in the gold-bearing mineralization at the Krasniy also has systematically higher content of radiogenic ^{206}Pb and ^{207}Pb. Another difference for these deposits are contrasting $^{207}Pb/^{206}Pb$ and $^{208}Pb/^{206}Pb$ ratios (the averages of 0.859 ± 2 (2SE) and 2.096 ± 4 (2SE) for Sukhoi Log; 0.847 ± 2 and 2.073 ± 5 for the Krasniy), but the latter are almost identical to Pb isotope signatures of sulfides from the Verninsky deposit (0.850 ± 2 and 2.074 ± 4). This is in a good agreement with the position of the host metasediments in the regional stratigraphy their position, i.e., the Aunakit Fm for the Krasniy and Verninsky deposits and underlying Khomolkho Fm for Sukhoi Log. Moreover, the ranges of Pb isotope ratios nearly entirely overlap in pyrite from the ore mineralization and that from barren rocks of the corresponding stratigraphy level (Fig. 14a). The calculation of model parameters for the Krasniy deposit indicates that Pb evolution proceeded in the source with heightened μ_2 and ω_2 relative to mid-crust values ($^{238}U/^{204}Pb$ = 9.92 ± 2 and $^{232}Th/^{204}Pb$ = 37.5 ± 5) and related to a supracrustal geochemical reservoir with increased values of U/Pb and Th/Pb ratios, e.g., marine sediments (e.g., Vlastélic et al., 2001). From this standpoint, the Pb supply into the mineral-forming system of the deposit should have been governed mostly by the host metasedimentary rocks. As summarized for the studied deposits of the Bodaibo region (Fig. 14), Pb isotope composition of sulfides results from mixing between the upper crustal and orogenic Pb, and reflects primary geochemical heterogeneity of the Neoproterozoic terrigenous-carbonate sequences of the Bodaibo region (Chugaev and Chernyshev, 2017;

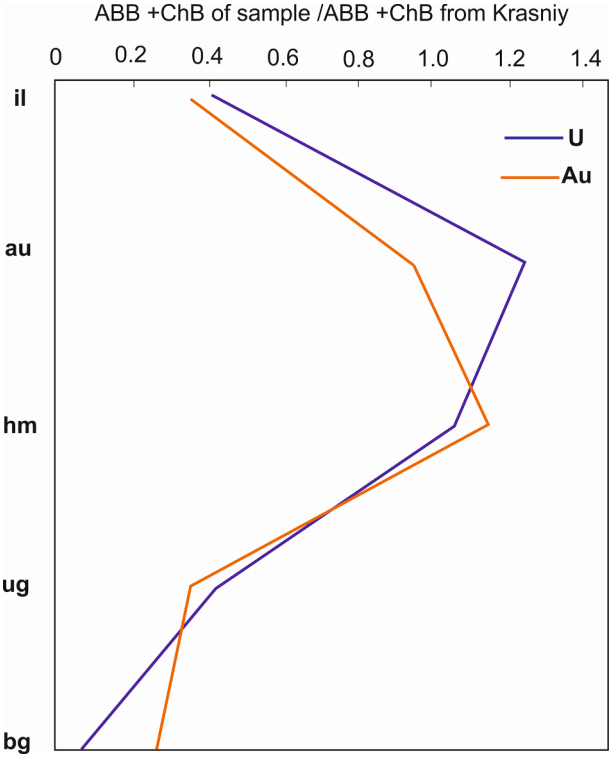

Fig. 20. Au and U concentrations in bitumens (ABB + CB) from the Neoproterozoic sediments of the Bodaibo region (analyzed by G.A.Vall at VSNIIGiMS). The values were normalized to Au and U contents of bitumens from the Krasniy ore zone (see Table 8). For the abbreviations of the corresponding formations see Fig. 2.

Chugaev et al., 2018). The upper part of the trend is occupied by the scattered points of pyrite from both gold-bearing mineralization and barren rocks from the Krasniy that emphasizes the role of hosting metasedimentary rocks as a primary source for mineralization. Given the fact of smaller Pb isotope variations that in Sukhoi Log and thus evidently more restricted volume of the involved host rocks and fluid circulation, the total Au resource of the Krasniy deposit yields both Sukhoi Log and Verninsky ones.

6.4. Towards a general model for the Sukhoi Log-type deposit formation

Considering a principal role of the host metasedimentary sequences as a primary metal source, the ore potential as well as formation and distribution of deposits should obey the same sequence of regional-scale geological events from the onset of black-shale sediment accumulation to their diagenetic, catagenic and metamorphic transformations (e.g., Budyak et al., 2016). More importantly, the scheme implies the concentration of gold and associated elements at each stage of epigenetic transformations (Fig. 22). The scheme displays three principal development stages of large gold deposits of the Sukhoi Log type in the southern Siberia: I – syn-sedimentary (sedimentation and diagenesis, 610–580 Ma), II – early collision (catagenesis, 570–540 Ma), III – collision (metamorphism, 450–420 Ma).

Stage I (sedimentation and diagenesis, 610–580 Ma). Sedimentation of the ore-bearing Khomolkho and Aunakit Fm with increased C_{org} occurred within a tilted back-arc basin gradually evolving into a foreland basin. The geochemical affinity of the host sedimentary sequences, particularly their original siderite-chalcophylle specialization and Au enrichment were linked to the hydrothermal activity of back-arc spreading and supply of the explosive material of the acting island-arc system (Nemerov and Stanevich, 2001; Budyak et al., 2016, Budyak et al., 2019). Synchronous to accumulation, diagenetic transformation of the sediments proceeded with microbiological sulphate reduction and formation of diagenetic (framboidal) pyrite-I, whereas the gold was bound both with dispersed mineralization (as seen from findings of gold in pyrite-I) and partially with clay and organic substance.

Stage II (catagenesis, 570–540 Ma). The onset of orogeny in the south due to accretion of the Baikal-Muya composite terrane (Skuzovatov et al., 2019a, Skuzovatov et al., 2019b) and a younger island-arc systems and microcontinental blocks (e.g., Donskaya et al., 2017; Gordienko and Metelkin, 2016) in the southern Siberia triggered tectonic stresses in the north as well as a sharp contraction of the sedimentation basin. This led to the gently-sloped folding and sediment transformation at the bottom section located in the north (Fig. 22). The erosion and denudation of the newly formed orogen was responsible for a supply of the molassa-like material into a sedimentary basin starting from the Anangrsky Fm (Yudoma group), which composed a thick cover on the sediments of the Dal'naya Taiga-Zhuya groups. As a result, the black shales of the Khomolkho and Aunakit Fm reached the conditions sufficient to trigger catagenetic transformations (T = 90–150° and P = 1–2 kb). This particular process might arguably correlate with the

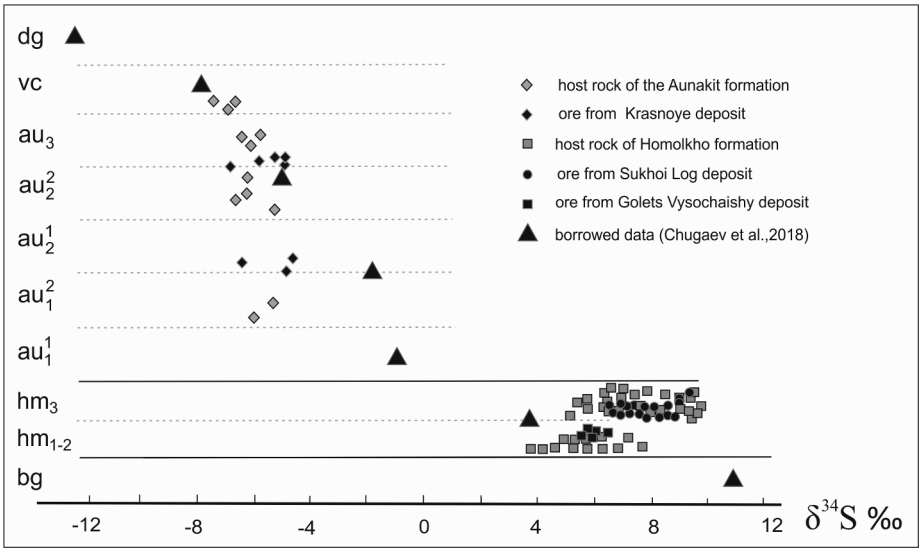

Fig. 21. Compilation of sulfur isotope composition of sulfides from Neoproterozoic sediments at the Bodaibo synclinorium (this work and literatures data). For the abbreviations of the corresponding formations see Fig. 2.

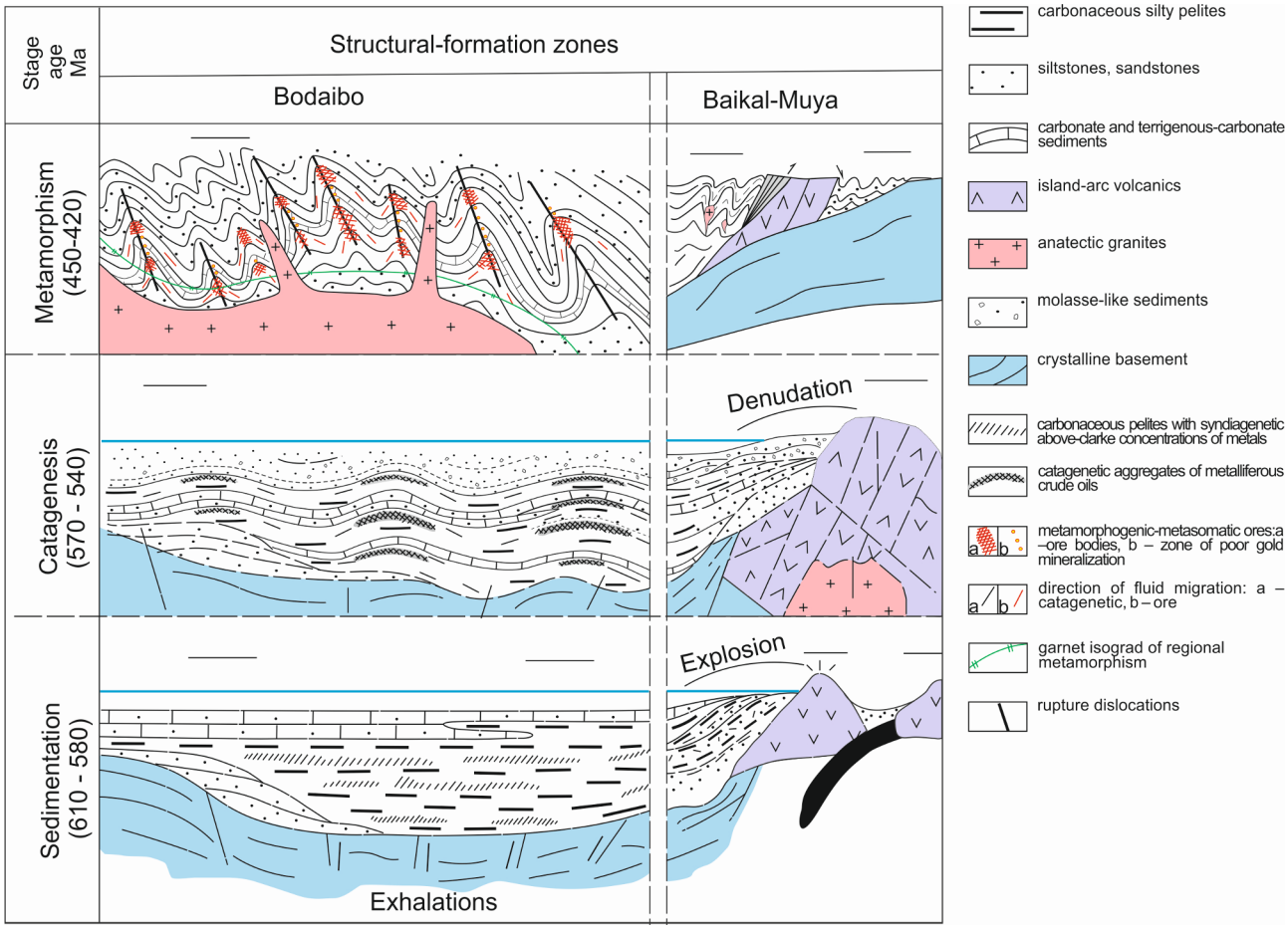

Fig. 22. Schematic model for the multi-stage formation of the Sukhoi Log-type gold deposits (modified by the authors from the originally proposed model of Nemerov et al., 2010).

age of metamorphic monazite from the sequences of the Dal'naya Taiga group (~570 Ma) (Meffre et al., 2008; Yudovskaya et al., 2011). Consequent migration of a catagenetic fluid into the hinge parts of gently-lying anticlines ensures the anomalous background of gold and formation of sulfide mineralization (pyrite-II).

Stage III (peak metamorphism, 450–420 Ma). This regional-scale stage of tectonic activity resulted in the intense folding, zonal metamorphism and anatectic granite formation of S-type (Zorin et al., 2008). During this major ore formation episode (Laverov et al., 2007; Meffre et al., 2008; Yudovskaya et al., 2011; Chugaev et al., 2014), the original ore associations were transformed as a response to gradual changes of P-T conditions.

Substage IIIa. While the temperature and pressure were growing to 300–380 °C and 5–6 kbar, respectively (greenschist-facies metamorphism; Petrov and Makrygina, 1975), the organic material in the apical parts of anticlines was carbonized and produced unstructured graphite. The decomposition of metalliferous crude oils led to release of water, carbonic acid, methane, hydrogen sulfide and free nitrogen, whereas gold and associated elements were unbound from the organic substance and partially dissolved in the CO_2-rich fluid. Their remnants transformed into native metals as nanoparticles and produced the dispersed mineralization in the rock volume, primarily in the native form or in the composition of solid metal solutions (Distler et al., 2004). This stage is marked by formation of high-T mineral association including pyrite-II, pyrrhotite-I, arsenopyrite-I, with calcite and quartz as gangue minerals. The associated syngenetic pore fluid represented by nitrogen of high density (to 0.53 g/cm^3), reported earlier by Distler et al. (2004) and Razvozzhaeva et al. (2007), most likely formed via decomposition of nitrogen-bearing organic compounds of the crude oils.

Substage IIIb. The high-T mineral association is replaced by low-T one (270–320 °C), with a considerable drop of pressure to 0.5 kb (Table 10). Such decompression could be caused by metamorphic transformations of substage *IIIa* and subsequent fracturing along the fold axes in the dehydrated sedimentary sequences. This process favored percolation of an acidic fluid (pH 3–4) (Distler et al., 2004) into the weak zones, thus forming the veinlet-impregnated mineral association III (Fig. 17) with sulfidation of high-T pyrrhotite-I to pyrite-III and low-Fe pyrrhotite-II, as well as appearance of the gold-bearing polymetallic mineral association.

Substage IIIc. While the system was evolving, the resultant acidic fluid became more neutral owing to the interaction with carbonate from the host sediments, and ore sedimentation became more low-T, with appearance of siderite-ankerite-quartz mineral association (Fig. 17) and minor amount of dispersed gold.

7. Conclusions

From the comprehensive studies conducted at the new, large-scale Krasniy deposit, as well as from accumulated background for the other well-known deposits of the Bodaido region (southern Siberia), large orogenic gold deposits of the Sukhoi Log-type occur in the certain stratigraphic groups of black-shale sequences within the Baikal-Patom Belt. The Khomolkho (Sukhoy Log and Golets Vysochaishy) and Aunakit (Verninsky, Nevsky and Krasniy) Fm hosting the largest gold deposits acquired their metalliferous and sidero-chalcophile specialization as well as high gold contents. Ore mineralization of orogenic gold deposits from BPP formed at the temperature of greenschist facies (200–400 °C). Thus, they are referred to the mesothermal type of

deposits (Sher, 1974). In general, the sequence of mineral associations formation in all orogenic gold deposits of the Sukhoi Log-type is similar. Framboidal pyrite-I and small idiomorphic crystals of pyrite-II with uniformly distributed nano-sized Au^0 formed at the earlier low temperature stage of diagenetic or catagenic transformations of host rocks. Mineral associations bearing arsenopyrite, pyrrhotite, pyrite-III, native gold, galena, chalcopyrite, sphalerite, fahl ores formed at the stage of greenschist metamorphism. Pyrite-IV in quartz-carbonate rim is derived from the post-ore stage. The available geochemical data suggests that in the formation of ore mineralization there was no any significant inflow of K, Na, Mg or Si. It is most likely that the ore-forming fluid for major gold-precipitating stage was generated in-situ and led only to redistribution of mineralization without changing the total balance of the components in host rocks. This evidence fits the hydrothermal models proposed for Sukhoi Log in the publications by (Buryak and Khmelevskaya, 1997; Large et al., 2007; Dubinina et al., 2014). The data on the S and Pb isotope composition in the Krasniy deposit sulfides points to a predominant supply of the ore components from the host Neoproterozoic metasedimentary sequences. This idea agrees with the supposition that metasedimentary sequences were the major substance, which contributed largely to formation of gold-bearing ore mineralization of the Sukhoi Log deposit (Chernyshev et al., 2009; Dubinina et al., 2014; Buryak and Khmelevskaya, 1997; Rusinov et al., 2008). The gold content over 1 ppm in bitumens from the metasedimentary rocks of Aunakit Fm indicates a potentially leading role of organic fluid in gold concentration and its redistribution throughout diagenetic and catagenic transformations. It is noteworthy that the gold ore mineralization of the Krasniy deposit has its own specific features, the major one being the abundant presence of arsenopyrite in the ores, which makes it distinct from the Sukhoi Log ores. This could be explained by the As abundance in the Aunakit black shales hosting the Krasniy deposit. The key distinction of the observed model from previously proposed ones (Buryak and Khmelevskaya, 1997; Large et al., 2007; Meffre et al., 2008) is the presence of pre-ore supply of gold and associated elements (Mo, U, V) through an organic fluid at the stage of catagenic transformations of hosting sediments.

Declaration of Competing Interest

The authors declare that they have no known competing financial interests or personal relationships that could have appeared to influence the work reported in this paper.

Acknowledgments

The manuscript has benefited much from the reviews of the two anonymous referees, whose effort is greatly acknowledged. We are indebted very much to Tatiana Bunaeva for translating the draft version of the manuscript. This work was carried out under state assignment Project IX.130.3.1. (0350-2019-0010). Lead isotope study was supported by Program no 8 of the Presidium of the RAS. Methods of stable isotope investigation were developed and supported under the state assignment of IGM SB RAS. The data reported in this paper were obtained on the equipment of the Central of Collective Use “Isotope-geochemical studies” (IGC SB RAS).

Appendix A. Supplementary data

Supplementary data to this article can be found online at https://doi.org/10.1016/j.oregeorev.2020.103365.

References

Barton Jr., P.B., Skinner, B.J., 1979. Sulfide mineral stabilities. In: Barnes, H.L. (Ed.), Geochemistry of hydrothermal ore deposits, second ed. John Wiley & Sons, New York, pp. 278–403.

Bodnar, R.J., Vityk, M.O., 1995. Interpretation of microtermometric data for H2O-NaCl fluid inclusions. In: Vivo, B. De, Frezzotti, M.L. (Eds.), Fluid Inclusions in Minerals, Methods and Applications. Virginia Tech., Blacksburg, VA, pp. 117–130.

Bogdanova, S.V., Pisarevsky, S.A., Li, Z.X., 2009. Assembly and breakup of Rodinia (some results of IGCP project 440). Stratigr. Geol. Corr. 17 (3), 259–274.

Brown, P., 1989. FLINCOR: a computer program for the reduction and investigation of fluid inclusion data. Am. Mineral. 74, 1390–1393.

Buchler, J.W., 1978. Syntheses and properties of metalloporphyrins. In: The Porphyrins. Academic Press Inc, pp. 389–483.

Budyak, A.E., 2009. Geochemical features of gold deposits paragenetically linked with black shale series (East Siberia). Thesis. Cand. Sci., 2009, 214 p. (in Russian).

Budyak, A.E., Bryukhanova, N.N., 2012. Selenium, bismuth, and mercury in black shale-hosted gold deposits of different genetic types. Geochem. Int. 50 (9), 791–797.

Budyak, A.E., Goryachev, N.A., Razvozzhaeva, E.A., Spiridonov, A.M., Sotskaya, O.T., Bryukhanova, N.N., 2015a. Geochemistry of dispersed organic matter in gold-ore deposits of black shale formations. Dokl. Earth Sci. 463 (6), 692–695.

Budyak, A.E., Parshin, A.V., Spiridonov, A.M., Volkova, M.G., Bryukhanova, N.N., Bryansky, N.V., Damdinov, B.B., Reutsky, V.N., 2015b. New results of geochemical and geophysical studies of the Khadatkandsky fault zone (North Trans-Baikal region). Russ. J. Pacific Geol. 9 (5), 373–380.

Budyak, A.E., Goryachev, N.A., Skuzovatov, S.Y., 2016. Geodynamic background for large-scale mineralization in the southern environs of the Siberian Craton in the Proterozoic. Dokl. Earth Sci. 470 (2), 1063–1066.

Budyak, A.E., Parshin, A.V., Spiridonov, A.M., Volkova, M.G., Tarasova, Y.I., Bryukhanova, N.N., Zarubina, O.V., Reutsky, V.N., Damdinov, B.B., Abramova, V.A., 2017. Geochemical controls of formation of unconformity-type Au–U deposits (Northern Trans-Baikal). Geochem. Int. 55 (2), 184–194.

Budyak, A.E., Skuzovatov, S.Yu., Tarasova, Yu.I., Wang, K.-L., Goryachev, N.A., 2019. Common Neoproterozoic-Early Paleozoic evolution of ore-bearing sedimentary complexes in the southern Siberian craton. Dokl. Earth Sci. 484 (1), 92–96.

Bukharov, A.A., Khalilov, V.A., Strakhova, T.M., Chernikov, V.V., 1992. Geology of the Baikal-Patom upland based on new data of U-Pb dating of accessory zircons. Russ. Geol. Geophys. 12, 29–39.

Buryak, V.A., Khmelevskaya, N.M., 1997. Sukhoi Log – One of the largest gold deposits in the world (Genesis, regularities in placing mineralization, and forecasting criteria). Dal'nauka, Vladivostok 156 (in Russian).

Buryak, V.A., Goncharov, V.I., Goryachev, N.A., 2002. Evolutionary series of large deposits of gold and platinum group metals in carbonaceous sequences. Dokl. Earth Sci. 387 (9), 1007–1009.

Chang, Z.S., Large, R.R., Maslennikov, V., 2008. Sulfur isotopes in sediment-hosted orogenic gold deposits: evidence for an early timing and a seawater sulfur source. Geology 36, 971–974.

Chernyshev, I.V., Chugaev, A.V., Shatagin, K.N., 2007. High-precision Pb isotope analysis by multicollector-ICP-mass-spectrometry using Tl-205/Tl-203 normalization: Optimization and calibration of the method for the studies of Pb isotope variations. Geochem. Int. 45 (11), 1065–1076.

Chernyshev, I.V., Chugaev, A.V., Safonov, Y.G., Saroyan, M.R., Yudovskaya, M.A., Eremina, A.V., 2009. Lead isotopic composition from data of high-precession MC-ICP-MS and sources of matter in the large-scale Sukhoi Log noble metal deposit, Russia. Geol. Ore Deposits 51 (6), 496–504.

Chugaev, A.V., Chernyshev, I.V., Lebedev, V.A., Eremina, A.V., 2013. Lead Isotope composition and origin of the quaternary lavas of Elbrus Volcano, the Greater Caucasus: High-precision MC-ICP-MS data. Petrology 21 (1), 16–27.

Chugaev, A.V., Plotinskaya, O.Yu., Chernyshev, I.V., Kotov, A.A., 2014. Lead isotope heterogeneity in sulfides from different assemblages at the Verninsky gold deposit (Baikal-Patom highland, Russia). Dokl. Earth Sci. 457 (1), 887–892.

Chugaev, A.V., Chernyshev, I.V., 2017. Pb–Pb isotopic systematics of orogenic gold deposits of the Baikal-Patom fold belt (Northern Trans-Baikal, Russia) and estimation of the role of Neoproterozoic crust in their formation. Geochem. Int. 55 (11), 1010–1021.

Chugaev, A.V., Budyak, A.E., Chernyshev, I.V., Shatagin, K.N., Oleinikova, T.I., Tarasova, Y.I., Skuzovatov, S.Y., 2017. Sources of clastic material of the Neoproterozoic metasedimentary rocks of the Baikal-Patom belt, Northern Trans-Baikal: evidence from Sm-Nd isotope data. Geochem. Int. 55 (1), 60–68.

Chugaev, A.V., Budyak, A.E., Chernyshev, I.V., Dubinina, E.O., Shatagin, K.N., Tarasova, Y.I., Skuzovatov, S.Y., Gareev, B.I., Goryachev, N.A., 2018. Isotopic (Sm–Nd, Pb–Pb, and $\delta^{34}S$) and geochemical characteristics of the metasedimentary rocks of the Baikal-Patom belt (Northern Transbaikalia) and evolution of the sedimentary basin in the Neoproterozoic. Petrology 26 (3), 213–245.

Chumakov, N.M., Semikhatov, M.A., Rudko, S.V., Kapitonov, I.N., Leonov, M.V., 2011. Vendian age of the upper part of the patom complex in Middle Siberia: U/Pb LA-ICP-MS dates of detrital zircons from the Nikolskoe and Zherba formations. Stratigr. Geol. Correl. 19 (2), 233–237.

Chumakov, N.M., Semikhatov, M.A., Sergeev, V.N., 2013. Vendian reference section of southern middle Siberia. 2013. Stratigraphy and Geological Correlation 21(4), 359–382.

Connolly, J.A.D., 2010. The mechanics of metamorphic fluid expulsion. Elements 6, 165–172.

Cox, S.F., 2016. Injection-driven swarm seismicity and permeability enhancement: implications for the dynamics of hydrothermal ore systems in high fluid-flux, overpressured faulting regimes - An invited paper. Econ. Geol. 111, 559–587.

Damdinov, B.B., Damdinova, L.B., Zhmodik, S.M., Mironov, A.G., 2019. Gold-bearing pyrrhotite ores in East Sayan: composition and formation conditions (by the example of the Ol'ginskoe ore occurrence). Russ. Geol. Geophys. 60 (5), 514–531.

Distler, V.V., Mitrofanov, G.L., Nemerov, V.K., 1996. Modes of occurrence of platinum group elements and their origin in the Sukhoi Log gold deposit. Geol. Ore Deposits 38

(6), 46–57.
Distler, V.V., Yudovskaya, M.A., Mitrofanov, G.L., Prokof'ev, V.V., Lishnevsky, E.N., 2004. Geology, composition, and genesis of the Sukhoi Log noble metals deposit, Russia. Ore Geology Reviews 24, 7–44.
Donskaya, T.V., Gladkochub, D.P., Fedorovsky, V.S., 2017. Pre-collisional (> 0.5 Ga) complexes of the Olkhon terrane (southern Siberia) as anecho of events inthe CentralAsian Orogenic Belt. Gondwana Res. 47, 228–248.
Dubinina, E.O., Chugaev, A.V., Ikonnikova, T.A., Avdeenko, A.S., Yakushev, A.I., 2014. Sources and fluid regime of quartz-carbonate veins at the Sukhoi Log gold deposit, Baikal-Patom Highland. Petrology 22 (4), 329–358.
Frei, R., Dahl, P.S., Frandsson, M.M., Jensen, L.A., Hansen, T.R., Terry, M.P., Frei, K.M., 2009. Lead-isotope and trace-element geochemistry of Paleoproterozoic metasedimentary rocks in the Lead and Rochford basins (Black Hills, South Dakota, USA): Implications for genetic models, mineralization ages, and sources of leads in the Homestake gold deposit. Precam. Res. 172, 1–24.
Fuchs, S., Schumann, D., Williams-Jones, A.E., Vali, H., 2015. The growth and concentration of uranium and titanium minerals in hydrocarbons of the Carbon Leader Reef, Witwatersrand Supergroup, South Africa. Chem. Geol. 393–394, 55–66.
Gladkochub, D.P., Stanevich, A.M., Mazukabzov, A.M., Donskaya, T.V., Motova, Z.L., Kornilova, T.A., Pisarevsky, S.A., Nicoll, G., 2013. Early evolution of the Paleoasian Ocean: LA-ICP-MS dating of detrital zircon from Late Precambrian sequences of the southern margin of the Siberian craton. Russ. Geol. Geophys. 54 (10), 1150–1163.
Gaboury, D., 2001. Predictive distribution of fault-fill and extensional veins: Example from the Sigma gold mine, Abitibi subprovince, Canada. Econ. Geol. Bull. Soc. Econ. Geol. 96 (6), 1397–1405.
Goldfarb, R.J., Baker, T., Duber, B., Groves, D.I., Hart, C.J.R., Gosselin, P., 2005. Distribution, character, and genesis of gold deposits in metamorphic terranes. In: Economic Geology and the Bulletin of the Society of Economic Geologists, One Hundredth Anniversary 1905, 407–450.
Gordienko, I.V., Mironov, A.G., 2008. Geodynamic and metallogenic evolution of the Baikal area in the Upper Riphean-Paleozoic. Otechestvennaya 3, 46–57 (in Russian).
Gordienko, I.V., Metelkin, D.V., 2016. The evolution of the subduction zone magmatism on the Neoproterozoic and Early Paleozoic active margins of the Paleoasian Ocean. Russ. Geol. Geophys. 57 (1), 69–81.
Groves, D.I., 1993. The crustal continuum model for late-Archaean lode-gold deposits of the Yilgarn Block, Western Australia. Mineral Deposits 28, 366–374.
Groves, D.I., Goldfarb, R.J., Gebre-Mariam, M., Hagemann, S.G., Robert, F., 1998. Orogenic gold deposits: a proposed classification in the context of their crustal distribution and relationship to other gold deposit types. Ore Geol. Rev. 13, 7–27.
Groves, D.I., Goldfarb, R.J., Gardoll, S., 2001. Orogenic gold and geologic time: a global synthesis. Ore Geol. Rev. 18, 1–75.
Groves, D.I., Goldfarb, R.J., Robert, F., Hart, C.J.R., 2003. Gold deposits in metamorphic belts: Overview of current understanding, outstanding problems, future research, and exploration significance. Econ. Geol. 98, 1–29.
Hall, A.J., 1986. Pyrite-pyrrhotite redox reactions in nature. Mineral. Mag. 50, 223–229.
Han, L., Tanweer, A., Szaran, J., Halas, S., 2002. A modified technique for the preparation of SO_2 from sulphates and sulphides for sulfur isotope analyses. Isotopes Environ. Health Studies 38 (3), 177–183.
Ivanov, A.I., 2014. Gold of Baikal-Patom (Geology, Mineralization, and Prospects). Central Research Institute of Geological Prospecting for Basic and Precious Metals Moscow, pp. 215 (in Russian).
Kalitkina, N.A., 1971. Study of the processes of coarsening and disintegration of gold in pyrite and arsenopyrite. Mosc. Univ. Geol. Bull. 5, 107–110 (in Russian).
Kazakevich, Yu.P., Sher, S.D., Zhadnova, T.P., 1971. Lena gold district. Stratigraphy, tectonics, magmatism and ore gold deposits, Moscow, 1971, 163 p. (in Russian).
Kerrich, R., Cassidy, K.F., 1994. Temporal relationships of lode gold mineralization to accretion, magmatism, metamorphism and deformation: Archean to present: a review. Ore Geol. Rev. 9, 263–310.
Kretschmar, U., Scott, S.D., 1976. Phase relations involving arsenopyrite in the system Fe-As-S and their application. Can. Mineral. 14, 364–386.
Kryazhev, S.G., Ustinov, V.I., Grinenko, V.A., 2009. Fluid regime at the Sukhoi Log gold deposit: isotopic evidence. Geochem. Int. 47 (10), 1041–1049.
Kucherenko, I.V., Gavrilov, P.Yu., Martynemko, V.G., Verhozin, A.V., 2012. Petrological and geochemical features of near-ore metasomatism from gold deposit Verninsky (Lena district). Bull. Tomsk Polytech. Univ. 321 (1), 22–33 (in Russian).
Kuznetsov, A.B., Ovchinnikova, G.V., Gorokhov, I.M., Letnikova, E.F., Kaurova, O.K., Konstantinova, G.V., 2013. Age constraints on the Neoproterozoic Baikal Group from combined Sr isotopes and Pb–Pb dating of carbonates from the Baikal type section, southeastern Siberia. J. Asian Earth Sci. 62, 51–66.
Large, R.R., Maslennikov, V.V., Robert, F., DanyushevskY, L.V., Chang, Z., 2007. Multistage sedimentary and metamorphic origin of pyrite and gold in the giant Sukhoi Log deposit, Lena Goldfield, Russia. Econ. Geol. 102, 1233–1267.
Large, R.R., Bull, S.W., Maslennikov, V.V., 2011. A carbonaceous sedimentary source-rock model for Carlin-type and orogenic gold deposits. Econ. Geol. 106, 331–358 DOI: 10.2113.
Laverov, N.P., Distler, V.V., Mitrofanov, G.L., Nemerov, V.K., Kovalenker, V.A., Mokhov, A.V., Semeikina, L.K., Yudovskaya, M.A., 1997. Platinum and other native metals in ores at the Sukhoi Log gold deposit. Dokl. Earth Sci. 355 (5), 664–667 (in Russian).
Laverov, N.P., Chernyshev, I.V., Chugaev, A.V., Bairova, E.D., Goltsman, Y.V., Distler, V.V., Yudovskaya, M.A., 2007. Formation stages of the large-scale noble metal mineralization in the Sukhoi Log deposit, East Siberia: results of isotope-geochronological study. Dokl. Earth Sci. 415 (1), 810–814.
Li, Z.X., Bogdanova, S.V., Collins, F.S., 2008. Assembly, configuration, and break-up history of Rodinia: a synthesis. Precambr. Res. 160 (1–2), 179–210.
Lishnevskii, E.N., Distler, V.V., 2004. Deep structure of the Earth's crust in the district of the Sukhoi Log gold-platinum deposit (Eastern Siberia, Russia) based on geological and geophysical data. Geol. Ore Deposits 46 (1), 76–90.
Manhes, G., Allegre, C.J., Provost, A., 1984. U-Th-Pb systematics of the eucrite juvinas - precise age-determination and evidence for exotic lead. Geochim. Cosmochim. Acta 48 (11), 2247–2264.
Manning, D.A.C., Gize, A.P., 1993. The role of organic matter in ore transport processes. In: Engel, M.H., and Macko, S.A. (eds.), Organic Geochemistry, 547–563.
Martikhaeva, D.Kh., Makrygina, V.A., Vorontsov, A.E., Razvozzhaeva, E.A., 2001. Carbonacecous substance in metamorphic and hydrothermal rocks./Novosibirsk. Publ. H. GEO 127 (in Russian).
Martynenko, V.G., Domashov, A.V., Deys, S.Yu., Korzakov, A.G., Kushnarev, P.I., 2017. The main features of the geological structure Verninsky gold deposit. Prospecting and protection of mineral resources 4, 3–8. (in Russian).
Meffre, S., Large, R.R., Scott, R., Scott, R., Woodhead, Z.C., Gilbert, S.E., Danyshevsky, L.D., Maslenikov, V.V., Hergt, J.M., 2008. Age and pyrite Pb isotopic composition of the giant Sukhoi Log sediment hosted gold deposit, Russia. Geochim. Cosmochim. Acta 72, 2377–2391.
Melezhik, V.A., Pokrovsky, B.G., Fallick, A.E., 2009. Constraints on $^{87}Sr/^{86}Sr$ of Late Ediacaran seawater: insight from Siberian high-Sr limestones. J. Geol. Soc. 166 (1), 183–191.
Neymark, L.A., Rytsk, E.Yu., Rizvanova, N.G., Gorokhovsky, B.M., 1993. On polychronous genesis of Angara-Vtim batolith according to U-Pb data on zircon and sphene. Dokl. Earth Sci. 333, 634–638 (in Russian).
Nemerov, V.K., Stanevich, A.M., 2001. Evolution of Riphean-Vendian environments of bio-lithogenesis of the Baikal mountain area. Russ. Geol. Geophys. 42 (3), 256–261.
Nemerov, V.K., Razvozzhaeva, E.A., Budyak, A.E., Stanevich, A.M., Kornilova, T.A., 2010. Biogenic sedimentation factors of mineralization in the Neoproterozoic strata of the Baikal-Patom region. Russ. Geol. Geophys. 51 (5), 572–586.
Palenova, E.E., 2015. Mineralogy of gold deposits Kopylovsky, Kavkaz, Krasny (Artem ore zone, Bodaybo district). Thesis. Cand. Sci., 2015 (in Russian).
Pal'yanova, G.A., Reutsky, V.N., Sobolev, E.S., Bortnikov, N.S., 2016. Upper Triassic pyritized bivalve mollusks from the sentachan orogenic gold–antimony deposit, Eastern Yakutia: mineralogy and sulfur isotopic composition. Geology of Ore Deposits 58(6), 456–464.
Palenova, E.E., Belogub, E.V., Plotinskaya, O. Yu., et al., 2015. Chemical evolution of pyrite at the Kopylovsky and Kavkaz black shale-hosted gold deposits, Bodaybo district, Russia: Evidence from EPMA and LA-ICP-MS data. Geol. Ore Deposits 57 (1), 64–84. https://doi.org/10.1134/S107570151501002X.
Palenova, E.E., Yudovskaya, M.A., Frei, D., Rodionov, N.V., et al., 2019. Detrital zircon U-Pb ages of Paleo- to Neoproterozoic black shales of the Baikal-Patom Highlands in Siberia with implications to timing of metamorphism and gold mineralization. J. Asian Earth Sci. 174, 37–58. https://doi.org/10.1016/j.jseaes.2018.10.022.
Petrov, B.V., Makrygina, V.A., 1975. Regional metamorphism and ultrametamorfism geochemistry. Nauka, Novosibirsk, pp. 341.
Phillips, G.N., Powell, R., 2010. Formation of gold deposits: a metamorphic devolatilization model. J. Metamorph. Geol. 28, 689–718.
Pokrovsky, B.G., Bujakaite, M.I., 2015. Geochemistry of C, O, and Sr isotopes in the Neoproterozoic carbonates from the southwestern Patom paleobasin, southern Middle Siberia. Lithol. Min. Resour. 50 (2), 144–169.
Powerman, V., Shatsillo, A., Chumakov, N., Kapitonov, I., Hourigan, J., 2015. Interaction between the Central Asian Orogenic Belt (CAOB) and the Siberian craton as recorded by detrital zircon suites from Transbaikalia. Precambr. Res. 267 (1), 39–71.
Razvozzhaeva, E.A., Nemerov, V.K., Makrygina, V.A., 2007. Carbon isotope composition of sedimentary rocks in the southern Siberian Platform and surrounding fold systems. Geochem. Int. 45 (3), 261–269.
Razvozzhaeva, E.A., Spiridonov, A.M., Tauson, V.L., Budyak, A.E., 2011. Modes of gold occurrence in carbonaceous shales at the Patom highland, Eastern Siberia. Geochem. Int. 49 (9), 942–948.
Razvozzhaeva, E.A., 2015. Geochemistry of carbon and noble metals from metasedimentary complexes at folded surrounding of the Siberian platform. Novosibirsk, Geo 135 (in Russian).
Rundquist, D.V., 1997. Time factor in the formation of hydrothermal deposits: periods, epochs, megastages, and stages of ore formation. Geol. Ore Deposits 39 (1), 8–19.
Rusinov, V.L., Borisovsky, S.E., Rusinova, O.V., Kryazhev, S.G., Shchegolkov, Yu.V., Alysheva, E.I., 2008. Wall-rock metasomatism of carbonaceous terrigenous rocks in the Lena gold district. Geol. Ore Deposits 50 (1), 1–40.
Safonov, Yu.G., 2003. Gold and gold-bearing deposits of the world: genesis and metallogenic potential. Geol. Ore Deposits 45 (4), 265–278.
Scott, S.D., Barnes, H.L., 1971. Sphalerite geothermometry and geobarometry. Econ. Geol. 66 (4), 653–669.
Scott, S.D., 1983. Chemical behaviour of sphalerite and arsenopyrite in hydrothermal and metamorphic environments. Mineral. Mag. 47, 427–435.
Scott, R.J., Large, R.R., Meffre, S., Masslenikov, V.V., 2007. Structural controls on the development of the giant Sukhoi Log gold deposit, Siberia: deformation in the desert. In: Geological Society of Australia, Specialist Group in Tectonics and Structural Geology, Alice Springs, 55.
Sher, S.D., 1974. Gold metallogeny. Nedra, Moscow, pp. 256.
Sibson, R.H., Robert, F., Poulsen, K.H., 1988. High-angle reverse faults, fluid-pressure cycling, and mesothermal gold-quartz deposits. Geology 16, 551–555.
Sillitoe, R.H., Thompson, J.F.H., 1998. Intrusion-related vein gold deposits: types, tectono-magmatic settings and difficulties of distinction from orogenic gold deposits. Resour. Geol. 48, 237–250.
Simmons, S.F., Brown, K.L., 2006. Gold in magmatic hydrothermal solutions and the rapid formation of a giant ore deposit. Science 314 (5797), 288–291.
Skuzovatov, S.Yu., Shatsky, V.S., Dril, S.I., Perepelov, A.B., 2018. Elemental and isotopic (Nd-Sr-O) geochemistry of eclogites from the Zamtyn-Nuruu area (SW Mongolia): crustal contribution and relation to Neoproterozoic subduction-accretion events. J.

Asian Earth Sci. 167, 33–51.
Skuzovatov, S.Yu., Shatsky, V.S., Wang, K.-L., 2019a. Continental subduction during arc-microcontinent collision in the southern Siberian craton: constraints on protoliths and metamorphic evolution of the North Muya complex eclogites (Eastern Siberia). Lithos 342–343, 76–96.
Skuzovatov, S.Yu., Wang, K.-L., Dril, S.I., Lee, H.-Y., Iizuka, Y., 2019b. Geochemistry, zircon U-Pb and Lu-Hf systematics of high-grade metasedimentary sequences from the South Muya block (northeastern Central Asian Orogenic Belt): reconnaissance of polymetamorphism and accretion of Neoproterozoic exotic blocks in southern Siberia. Precambr. Res. 321, 34–53.
Stanevich, A.M., Maksimova, E.N., Kornilova, T.A., Mazukabzov, A.M., Gladkochub, D.P., 2007a. Microfossils of the Late Proterozoic Debengdinskaya formation of the Olenekskiy uplift. Bull. Tomsk Polytech. Univ. 311 (1), 9–13 (in Russian).
Stanevich, A.M., Mazukabzov, A.M., Gladkochub, D.P., Donskaya, T.V., Kornilova, T.A., Postnikov, A.A., Nemerov, V.K., Pisarevsky, S.A., 2007b. Northern segment of the Paleoasian ocean: Neoproterozoic deposition history and geodynamics. Russ. Geol. Geophys. 48 (1), 46–60.
Sugiyama, I., 2015. Metal transport by oil: application to ore Genesis. Earth and Planetary Sciences, McGill University Montréal Quebec, M.Sc. Thesis.
Tauson, V.L., Chernyshev, L.V., 1981. Experimental Studies on The Crystal Chemistry Of Zinc Sulfide. Nauka, Novosibirsk, pp. 190.
Tauson, V.L., 1999. Gold solubility in the common gold-bearing minerals: Experimental evaluation and application to pyrite. Eur. J. Mineral., vol 11. N6, P.937-947.
Tauson, V.L., Nemerov, V.K., Razvozzhaeva, E.A., Spiridonov, A.M., Lipko, S.V., Budyak, A.E., 2009. Paragenetic relationships between pyrite, carbon, and gold at the Sukhoi Log deposit and typomorphism of the pyrite surface. Dokl. Earth Sci. 426 (1), 690–694.
Tauson, V.L., Pastushkova, T.M., Babkin, D.N., Krasnoshchekova, T.S., Lustenberg, E.E., 2010. The effect of the crystal size in sample on the trace-element concentration. Russ. Geol. Geophys. 51 (7), 764–773.
Tauson, V.L., Akimov, V.V., Lipko, S.V., Spiridonov, A.M., Budyak, A.E., Belozerova, O.Yu., Smagunov, N.V., 2015. Typomorphism of pyrite of the Sukhoi Log deposit (East Siberia). Russ. Geol. Geophys. 56 (10), 1394–1413.
Tomkins, A.G., 2010. Windows of metamorphic sulfur liberation in the crust: implications for gold deposit genesis. Geochim. Cosmochim. Acta 74, 3246–3259.
Torgov, V.G., Khlebnikova, A.A., 1977. Atomic absorption determination of gold in a flame and flameless graphite analyzer with preliminary isolation by extraction with oil sulfides. J. Anal. Chem. 32 (5), 960–964.
Toulmin III, P., Barton Jr., P.B., 1964. A thermodynamic study of pyrite and pyrrhotite. Geochim. Cosmochim. Acta 28 (5), 641–671.
Tsygankov, A.A., Posokhov, V.F., Tsyrenov, B. Ts., Khromov, A.A., Matukov, D.I., Berezhnaya, N.G., Larionov, A.N., Sergeev, S.A., 2007. Late Paleozoic granitoids of Western Transbaikalia: magma sources and stages of formation. Russ. Geol. Geophys. 48 (1), 120–140.
Tsygankov, A.A., Litvinovsky, B.A., Jahn, B.M., Reichow, M.K., Liu, D.Y., Larionov, A.N., Presnyakov, S.L., Lepekhina, Y.N., Sergeev, S.A., 2010. Sequence of magmatic events in the Late Paleozoic of Trans-Baikal region, Russia (U-Pb isotope dating). Russ. Geol. Geophys. 51 (9), 972–994.
Vagina, E.A., 2012. Fluid inclusion compositions of gold deposit Chertovo Koryto. In: Proceedings of XV Russian Conference of thermobarogeochemistry, Moscow, IGEM RAS, 2012, p. 23-24. (in Russian).
Vall G.A., Voropaeva E.V., 1982. Direct atomic-absorption determination of metallic impurities in soluble media. Certificate of authorship SU 1337760 A1. USSR №1087848, G 01№21/73. (in Russian).
Varshalll, G.M., Veluhanova, T.K., Kosheeva, I.Ya., Baranova, N.N., Kozerenko, S.V., Galuzinskaya, A.H., Safronov, N.S., Bannyh, L.N., 1994. About concentration noble metals by organic matter from rocks. Geochem. Int. 6, 814–824 (in Russian).
Vilor, N.V., Kazharskaya, M.G., Bychinskii, V.A., Kostyanetskaya, Zh.V., Men'shikov, V.I., Baranov, V.A., 2003. Geochemical correlations and the dynamics of solution-rock relations in mineralized fluid systems. Geochem. Int. 41 (12), 1194–1206.
Vinogradov, V.I., Pichugin, L.P., Byhover, V.N., Golovin, D.I., Murav'ev, V.I., Byyakaite, M.I., 1996. Isotopic features and age of epigenetic transformations upper Precambrian sequences from Urin upload. Lithology and Mineral Resources 1, 68–78. (in Russian).
Vlastélic, I., Abouchami, W., Galer, S.J.G., Hofmann, A.W., 2001. Geographic control on Pb isotope distribution and sources in Indian Ocean Fe-Mn deposits. Geochim. Cosmochim. Acta 65 (23), 4303–4319.
Wood, B.L., Popov, N.P., 2006. The giant Sukhoi Log gold deposit. Russ. Geol. Geophys. 47, 315–341.
Yapaskurt, O.V., 2005. The aspects of the post-sedimental lithogenesis theory. Lithosphere 3, 3–30.
Yarmolyuk, V.V., Budnikov, S.V., Kovalenko, V.I., Antipin, V.S., Goreglyad, A.V., Sal'nikova, E.B., Kotov, A.B., Kozakov, I.K., Kovach, V.P., Yakovleva, S.Z., Berezhnaya, N.G., 1997. Geochronology and geodynamic setting of the Angara-Vitim batholith. Petrology 5 (5), 401–414.
Yudovskaya, M.A., Distler, V.V., Mokhov, A.V., Rodionov, N.V., Antonov, A.V., Sergeev, S.A., 2011. Relationship between metamorphism and ore formation at the Sukhoi Log gold deposit hosted in black slates from the data of U-Th-Pb isotopic SHRIMP-dating of accessory minerals. Geol. Ore Deposits 53 (1), 27–57.
Yudovskaya, M.A., Distler, V.V., Prokofiev, V.Yu., Akinfiev, N.N., 2016. Gold mineralization and orogenic metamorphism in the Lena province of Siberia as assessed from Chertovo Koryto and Sukhoi Log deposits. Geosci. Front. 7 (3), 453–481.
Zhmodik, S.M., Postnikov, A.A., Buslov, M.M., Mironov, A.G., 2006. Geodynamics of the Sayan-Baikal-Muya accretion-collision belt in the Neoproterozoic-Early Paleozoic and regularities of the formation and localization of precious-metal mineralization. Russ. Geol. Geophys. 1, 183–197.
Zhong, R., Brugger, J., Tomkins, A.G., Chen, Y., Li, W., 2015. Fate of gold and base metals during metamorphic devolatilization of a pelite. Geochim. Cosmochim. Acta 171, 338–352.
Zorin, Yu.A., Mazukabzov, A.M., Gladkochub, D.P., 2008. The Silurian age of the major orogenic deformations of Riphean rocks in the Baikal-Patom zone. Dokl. Earth Sci. 463 (2), 1235–1239.